Mine Water and the Environment (2024) 43:340–367
https://doi.org/10.1007/s10230-024-00989-z

TECHNICAL ARTICLE

A Review of Viable Mineral Precipitates in Pit Lake Modeling

Andy Davis[1] · **M. Lengke**[1] · **N. Sims**[1] · **M. Roth**[1]

Received: 28 November 2023 / Accepted: 20 May 2024 / Published online: 3 July 2024

Abstract
Mine permitting requires an analysis of reasonably foreseeable impacts. In pit lake models, precipitates may be invoked to reduce dissolved aqueous concentrations, and thereby perceived groundwater impacts in the event of a throughflow pit lake after mine closure. The phases selected by modelers are generally based on geochemical theory rather than empirical data, and in this context, a review of available information is helpful. The mineralogy of Spanish, German, Czechian, Australian, and USA acidic pit lakes includes schwertmannite, jarosite, alunite, amorphous ferric oxyhydroxide (AFH), ferrihydrite, goethite, hydrobasaluminite, gibbsite, amorphous iron and aluminum oxyhydroxysulfates, gypsum, barite, and clays (kaolinite, dickite, halloysite, and smectite). Conversely, alkaline pit lakes exhibit distinct inorganic precipitation of calcite, ikaite, gaylussite, and siderite entraining metal removal from solutions at pH > 7 with biogenic iron oxyhydroxides and carbonates. Microbial activity facilitates the formation and transformation of metal sulfide precipitates predominantly in alkaline pit lakes but also in acidic water bodies. Therefore, predictive pit lake studies should focus on selecting authigenic precipitates on an empirical basis where possible, or if observed in corresponding environments in the case of permitting a new pit lake, taking into consideration kinetic barriers to mineral precipitation. This study characterized amorphous iron, aluminum, and calcium precipitate with entrained arsenic, manganese, and zinc floc from the previously acidic, now alkaline Lone Tree pit lake. The formerly acidic Liberty pit lake generated primarily gypsum and AFH, while the basic former Cortez pit lake sediment comprised calcite with solid solution Ba, Cd, Mg, Mn, and Zn.

Keywords Precipitates · Geochemical modeling · Titration · Mineral solubility

Introduction

Modeling the fate and transport of metals in mine settings has become an important issue because analysis of pit lake chemistry, pit backfill pore water, and waste rock drain down is required as an integral part of contemporary mine permitting (NDEP 2022) that may have substantial economic repercussions if the model results are aberrant. These models invariably invoke precipitates, e.g. amorphous ferric hydroxide [AFH or $Fe(OH)_3$]; ferrihydrite; gibbsite [$Al(OH)_3$]; gypsum [$CaSO_4{\cdot}2H_2O$], etc. This is an important issue because the consequence is decreased dissolved solute concentration that may underestimate environmental impacts.

At the baseline study level, a pit lake prediction is required prior to mine development if the mine goes far enough below the groundwater table that backfilling is not economically viable. In this case, there is reliance on the geochemical literature (e.g. Eary 1999) to select potential precipitating phases. For existing pit lakes requiring an update to the mine water pollution control permit (necessary to continue operations), data paucity should be less of a problem because in situ precipitate traps can be deployed, e.g. Sánchez-España et al. (2012, 2016), or opportunistic precipitates collected, e.g. from a rope dangling in the Berkeley pit lake for many years (Gammons and Duaime 2006).

Aqueous floc typically consists of microscopic particles, usually mixed colloids that require advanced filtration equipment to obtain samples. Subsequent analysis to adequately characterize the material generally includes X-ray diffraction (XRD), scanning electron microscope (SEM), field emission SEM and electron microprobe analysis (EMPA). However, methods to determine whether trace elements are sorbed or part of the colloid structure are inexact, expensive, and time-consuming.

✉ Andy Davis
andy@geomega.com

[1] Geomega, 2585 Central Ave, Boulder, CO 80301, USA

From a regulatory perspective in the USA, modeling pit lakes requires integration of the results of outflow from the recovering groundwater into the pit with the wall rock reactivity of the ultimate pit surface. Aqueous geochemical reactions invoking precipitating solids are superimposed on the resulting total metal chemistry and removed from the model to represent floc settling to the base of the pit lake (Fig. 1a). In this case, throughflow pit lakes are represented by the dissolved chemistry, which is compared with regulatory standards to determine the potential impacts on adjacent downgradient groundwater. Hence selection of an unrealistic set of precipitates will result in an underestimation of the aqueous chemical concentrations, and potential impacts. In contrast, the total predicted water quality (precluding precipitate formation) is required for a screening level ecological risk assessment (SLERA) of the pit lake, based on the concept that biota accessing the water will also consume the precipitates (NDEP 2021).

If pits are backfilled with waste rock prior to recovery of the groundwater surface (Fig. 1b), it is necessary to understand the evolving pore water chemistry as the ground water table rebounds, resulting in saturated backfill. In the case of

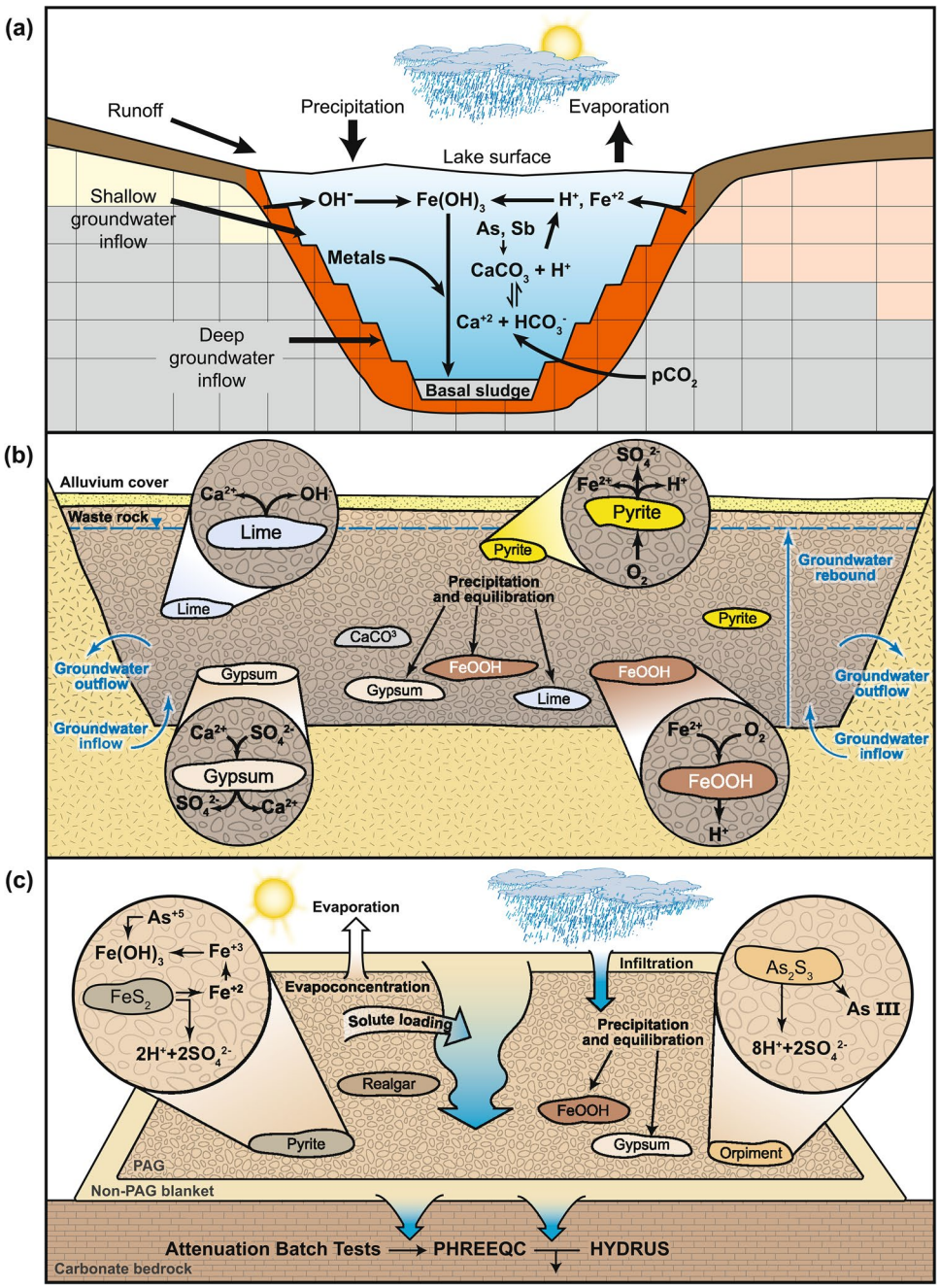

Fig. 1 A consortium of reactions anticipated to control major ion and trace metal solubility in (**a**) pit lakes, (**b**) backfilled pits, and (**c**) waste rock disposal facilities

throughflow pits, hydrologic equilibrium is re-established as groundwater recovers after mining ends and the hydraulic gradient is restored. Therefore, pore water chemistry is usually compared with groundwater drinking standards. Invoking unreasonable precipitates in the model will reduce the pore water solute concentrations, and again, the apparent impact on surrounding groundwater.

Finally, waste rock disposal facility (WRDF) draindown modeling can also invoke precipitates in the underlying vadose zone, resulting from the interaction of percolating precipitation with the waste rock and subjacent alluvium or bedrock (Fig. 1c). In this case, a mineral consortium can be selected to mitigate the draindown chemistry below the WRDF, and attenuation invoked in alluvium/bedrock prior to reaching groundwater. All these geochemical models require assumptions as to the precipitating phases allowed to control metal solubility that intrinsically affect the results, and consequently, any perceived environmental impacts.

Pit Lake Models

Newman (2020), in a review of nine pit lake studies, demonstrated the disparate selection of solid-phase precipitates. He also pointed out that this was the area of most variability, and that direct evidence as to the abundance of the phases in most of the pit lakes was lacking.

The subject has also been the topic of regulatory input. For example, the Nevada Division of Environmental Protection (NDEP 2021) guidance for geochemical modeling at mine site's states that "*The principles of thermodynamics are used to calculate mineral saturation indices." However, thermodynamic calculations do not account for processes that may preclude or retard precipitation, such as kinetic barriers, residence time of water in the reservoir of interest, and various other factors* (Nordstrom 2009). NDEP (2021) concluded, "*These factors may mean that although mineral precipitation is thermodynamically favored, precipitation may not necessarily occur.*"

Consequently, it is incumbent on the pit lake practitioner to select mineral precipitates that can be shown to be specific to the locale, kinetically feasible, and thermodynamically stable. This paper represents a step towards initiating a dialog on the appropriate phases used to model these complex systems.

Acidic Pit Lakes

Acidic pit lakes represent a unique environmental phenomenon, often stemming from post-mining operations in sulfide-rich and lignite mine areas. They are characterized by their acidity, elevated sulfate (SO_4) levels, and metal content.

Lausitz, Mitteldeutschland, and Oberpfalz Pit Lakes, Germany

The pH in 18 German lignite mine acidic pit lakes ranging from 7 to 45 m deep and 3–40 years after flooding (Lausitz, Mitteldeutschland, and Oberpfalz) ranged from 2.7 to 4.7 (Regenspurg et al. 2004). They contained variable SO_4 (307–1862 mg/L), Fe (< 0.06–624 mg/L), and Al (< 2.7–213 mg/L).

FTIR spectroscopy confirmed schwertmannite, first identified nominally as $Fe_8O_8(OH)_6(SO_4)\cdot nH_2O$ by Bigham et al. (1996) in the colloid fraction (1–10 kDa) of three of the lake surface waters. It was also found in the upper (1–5 cm) sediment layers of 16 of the lakes, with secondary confirmation in five of the lakes using XRD, FTIR, and the Fe:S ratio in the oxalate extractable fraction. The black layers with an H_2S odor in two acidic Lausitz pit lake sediment samples were associated with microbially mediated SO_4 and Fe(III) reduction (Meier et al. 2004).

Schwertmannite was also identified as the initial precipitate following oxidation and hydrolysis of slightly acidic (pH 5–6), Fe(II)–SO_4 solutions. Stability experiments demonstrated that synthetic schwertmannite transformed into goethite more rapidly with increasing pH.

Aerodrome and Twin Lakes, Western Australia

These lakes are among numerous ephemeral acid saline lakes in Western Australia (Story et al. 2010). XRD and SEM of silt- and clay-size sediments identified complex and spatially heterogeneous mineral assemblages, including authigenic phyllosilicates (e.g. kaolinite, dickite, halloysite, and smectite), sulfates (e.g. alunite, jarosite, gypsum, rozenite, hydrobasaluminite), Fe-oxides (e.g. hematite and goethite), other silicates (anatase and mullite), and gibbsite.

Berkeley Pit Lake, Montana, USA

This hard rock pit lake in Butte, Montana has dominant SO_4, major ions, and Cu, Mn, and Zn in the hundreds of mg/L. In the spring at ice-out, the pit lake was green (Fe 386 mg/L, SO_4 5,740 mg/L; Davis and Ashenberg 1989), indicative of $Fe^{2+}SO_{4\,(aq)}$; however, with oxygen entrainment the water quickly became turbid and brown, probably because of oxidation to AFH. Sediment collected on filters from different depths was approximately $AlCaFe(SO_4)$ with lesser amounts of Cu, K, Mn, and Zn at the surface (pH 2.8), while at 100 m where the pH was 3.1 (34 m above the base of the pit), the elemental concentrations approximately doubled but had a similar stoichiometry.

While no mineralogic analysis was undertaken, the authors proposed that based on modeling, that possible mineral controls might include $Fe(OH)_3$, gypsum ($CaSO_4\cdot 2H_2O$),

jurbanite ($AlOHSO_4$) and jarosite [$KFe_3(SO_4)_2(OH)_6$]. Gammons and Duaime (2006) partially confirmed this assemblage through a XRD analysis of floc from the water column that, consistent with the model results, indicated coprecipitation of jarosite and schwertmannite in the Berkeley pit lake profile. Twidwell et al. (2006) also identified jarosite and gypsum precipitation, albeit from the basal sediments of Berkeley pit lake. It is likely that jurbanite could not be confirmed because Bigham and Nordstrom (2000) discredited the importance of this mineral due to its solubility.

Jones et al. (2011) used X-ray absorption near edge structure (XANES) to demonstrate that the solubility of Al draining from acid sulfate soils in New South Wales, Australia was controlled by amorphous $Al(OH)_3$ and basaluminite [$Al_4(SO_4)(OH)_{10}{\cdot}5H_2O$], rather than jurbanite. Aluminum could occur as a mixture of Al^{3+} adsorbed on schwertmannite surfaces and/or coprecipitated in jarosite, processes that may contribute to a reduction in dissolved Al^{3+} in acidic pit lakes, even at pH 3.5, as observed in the San Telmo pit lake, Spain (Sánchez-España et al. 2016).

Nordstrom (1982) noted that members of the alunite group [e.g. $KAl_3(SO_4)_2(OH)_6$] precipitate at low pH (< 4.0) in oxidizing environments, transforming to gibbsite [$Al(OH)_3$] as the stable phase above this threshold. van Breeman (1973, 1976) proposed that a stoichiometric 1:1:1 ratio of Al:OH:SO_4 controlled Al solubility in 127 acid mine waters.

Iberian Pyrite Belt Pit Lakes, Spain

The 21 Iberian Pyrite Belt (IPB) pit lakes, ranging in pH from 1.2 to 4.7 (Sánchez-España et al. 2008) are extremely diverse in size, depth, age, and water composition, but share a common geological framework and a chiefly meromictic lake stratification (Sánchez-España et al. 2009). The 15–80 m deep San Telmo, Confesionarios, Cueva de la Mora, Concepcion, Filon Centro, and Ntra. Sra. del Carmen pit lakes are meromictic and have a distinct chemocline, separating an anoxic, Fe(II)-rich monimolimnion from an oxygenated, Fe(III)-rich mixolimnion (Sánchez-España et al. 2009). In contrast, the Aznalcollar pit lake is holomictic with seasonal stratification and winter turnover (Sánchez-España et al. 2008).

While the surface waters exhibit relatively low SO_4 (0.9–32 mg/L), metals are elevated, i.e. Fe (0.4–36,675 mg/L), Al (4–1,919 mg/L), Mn (3–187 mg/L), with soluble trace metals including As, Cu, Cd, Co, Cr, Ni, Pb, and Zn. These chemical compositions are indicative of the oxidative dissolution of pyrite, other sulfides, and gangue aluminosilicates.

In the IPB pit lakes, schwertmannite precipitation in shallow water columns or sediments acts as a strong buffering mechanism, generating colloids that effectively adsorb trace metals from the surrounding aqueous solutions (Diez-Ercilla et al. 2019; Sánchez-España et al. 2005a, b, 2008, 2009). Sánchez-España et al. (2016) also observed the presence and formation of discrete, submicron alunite, as well as the abundance and distribution of Al within Fe(III) phases such as schwertmannite and jarosite, at a nanometric resolution. They inferred that the fate and transport of Al at low pH (< 4) can be substantially affected by adsorption on, and/or coprecipitation with both schwertmannite and jarosite.

Alunite is also unstable within this low pH range relative to jarosite, potentially leading to either isomorphic transformation, and/or the formation of chemically zoned crystals with jarositic rims surrounding previously formed alunite cores. The combination of this macroscopically invisible Al incorporated into Fe(III) solids alongside subordinate alunite formation may result in substantial Al removal, even at extremely low pH levels. Diez-Ercilla et al. (2019) noted the occurrence of schwertmannite, jarosite, and amorphous Al (amorphous hydrobasaluminite) at pH > 4, subsequently transforming into more crystalline basaluminite during sediment compaction and early diagenesis.

The Herrerias I (Guadiana) and Filon Centro pit lakes typically feature a thin chemocline separating an oxygen-saturated mixolimnion with low pH from a deeper, anoxic zone (Diez-Ercilla et al. 2014, 2019). The presence of secondary sulfides, predominantly covellite ($CuS_{(s)}$) and micro-crystalline sphalerite ($ZnS_{(s)}$) in the Filon Centro monimolimnion is indicative of biogenic sulfide formation by sulfate-reducing bacteria (SRB). This was corroborated by microbial diversity analysis through 16S rRNA gene amplicon sequencing of water column samples that identified sulfidogenic microbial taxa in both the Filon Centro and La Zarza pit lakes (van der Graaf et al. 2020).

Brunita Pit Lake, Spain

The pit lake pH ranges from 2.2 (0–12 m) to 5.0 (> 12–24 m), with elevated Fe (500–6400 mg/L), SO_4 (26,000–38,400 mg/L), Mn (up to 2000 mg/L), Zn (500 mg/L), Cu (250 mg/L), Mg (5500 mg/L), Cl (750–1300 mg/L), Na (300–630 mg/L) and high salinity (58‰) at the base, forming a meromictic condition where an anoxic, reducing monimolimnion is isolated from the oxygenated mixolimnion. Metal removal in the monimolimnion, including Cu, Zn, Cd, Cr, Pb, and Th, may occur through interaction with biogenic H_2S and subsequent precipitation as metal sulfides. SEM identified submicron, spherical ZnS particles associated with cocci and rod-shaped bacteria (Sánchez-España et al. 2020).

Jiri and Lomnice Pit Lakes, Czechia

The Jiri pit lake is acidic (2.3–3.2) with elevated Fe (25 mg/L) and SO_4 (> 1600 mg/L), while the Lomnice is also acidic (pH 3.2). XRD and transmittance infrared (IR) identified schwertmannite, goethite, and jarosite precipitating in the Jiri pit lake, whereas only schwertmannite and goethite were identified in the Lomnice area, but not within the pit lake itself (Murad and Rojik 2005).

Alkaline Pit Lakes

Alkaline pit lakes (pH > 7) promote carbonate precipitation in the water column, complexing elements with a similar ionic radius.

Medard Pit Lake, Czechia

Following closure of the lignite mine, the pit lake has a stratified water column with stable temperature, ORP, and salinity profiles throughout the year. The pH in the hypolimnion was 8.2, decreasing to 7.4 near the anoxic surface water interface (Petrash et al. 2022). The conductivity declined sharply at 48 m, with the subjacent salinity tripling, possibly due to groundwater recharge.

The pit lake becomes anoxic below 49 m, consistent with the ORP shift from positive in the lower mixolimnion to negative values near the sediment–water interface, accompanied by an increase in SO_4 and dissolved Fe(II). Below 54 m, Fe decreases by ≈ 14%, attributed to the coprecipitation of Fe(II) and S as metastable FeS. The lower monimolimnion exhibits increased SO_4 reduction activity, correlated with increased taxonomic diversity and relative abundances of SRB (Petrash et al. 2022).

The anoxic sediments contain predominantly goethite and lepidocrocite, along with clay, chalcedony, and trace pyrite based on XRD and XANES (Petrash et al. 2018) with the iron minerals intertwined with organic matter, suggesting SRB involvement. High levels of Si, C, and P were also detected in iron-rich spherical structures, with P associated with Ca-bearing precipitates and potentially Al-hydroxides.

Metastable Fe(III) oxyhydroxides and oxyhydroxysulfates precipitate, facilitated by both abiotic and microbial processes, particularly near the pelagic redoxcline. These precipitates are subsequently exported to the sediment–water interface (Petrash et al. 2018).

Mono Lake, California, USA

This is a hypersaline, alkaline lake, characterized by a Na–CO_3–Cl–SO_4 brine resulting from evapoconcentration of inflowing water, weathering of surrounding rocks, and mineral precipitation (Council and Bennett 2015; Li et al. 1997). Initially meromictic in 1983, due to increased freshwater input, it transitioned to monomictic in 1989. Carbonates in the lake sediments, both inorganic and biogenic, include recently precipitated ikaite ($CaCO_3 \cdot 6H_2O$), minor gaylussite [$Na_2Ca(CO_3)_2 \cdot 5H_2O$], and calcite (Council and Bennett 2015).

Trace Metal Adsorption by Mineral Precipitates

The removal of solutes by amorphous Fe(III) hydroxide and ferrihydrite precipitation is an important process that controls the solubility of many metals (Drever 1982). Cations (e.g. Cd, Cu, Pb, and Zn) in solution may subsequently be sorbed or co-precipitated with Fe oxyhydroxide at pH > 5 (Dzombak and Morel 1990; Smith 1991; Swallow et al. 1980), while anionic species [e.g. As, Cr(VI), Mo, Se] are strongly sorbed to AFH at pH < 7.5 (Leckie et al. 1980). Precipitation and settling of Fe oxyhydroxide through the water column sequester solutes from solution, eventually entombing them within a metal-rich sludge (Fig. 2a) at the base of the pit (Miller et al. 1996). In addition, AFH, ferrihydrite, and other compounds such as schwertmannite, alunite, hydrobasaluminite, other Al hydroxides, and carbonates can also sorb or coprecipitate metals (Acero and Hudson-Edwards 2022; Chiarello et al. 1997; Cherniak 1997; Davis et al. 1987; Paquette and Reeder 1995; Reeder 1996; Papadopolous and Rowell 2006; Sánchez-España et al. 2016).

Carbonate precipitates incorporate other elements into their structure due to similar ionic radii, thereby removing them from the pit lake. For example, Ba, Co, and Zn (Reeder 1996), Cd (Chiarello et al. 1997; Davis et al. 1988; Reeder 1996), Mn (Paquette and Reeder 1995), Sr (Cherniak 1997; Paquette and Reeder 1995), and Pb (Cherniak 1997) have all been shown to be incorporated into $CaCO_3$ as a solid solution. Cadmium is particularly prone to this mechanism (Papadopoulos and Rowell 2006) because the ionic radius of Cd in the hexa-coordinated state (95 pm) is similar to that of Ca (100 pm).

The phases found to precipitate together with ancillary adsorption reactions provide a basis to select a reasonable solid assemblage with trace metal solubility controls for pit lake models. Once the mineral assemblage has been identified, another decision that must be made is the selection of the solubility product (log K_{sp}), which indicates the degree to which a solid dissociates in solution. This is an important consideration because aging of initial amorphous precipitates results in a more crystalline structure. For example, Yee et al. (2006) found rapid transformation of ferrihydrite to goethite facilitated by Fe^{2+}, while amorphous $Al(OH)_3$ ages to bayerite and finally, gibbsite (Koubeck 1999).

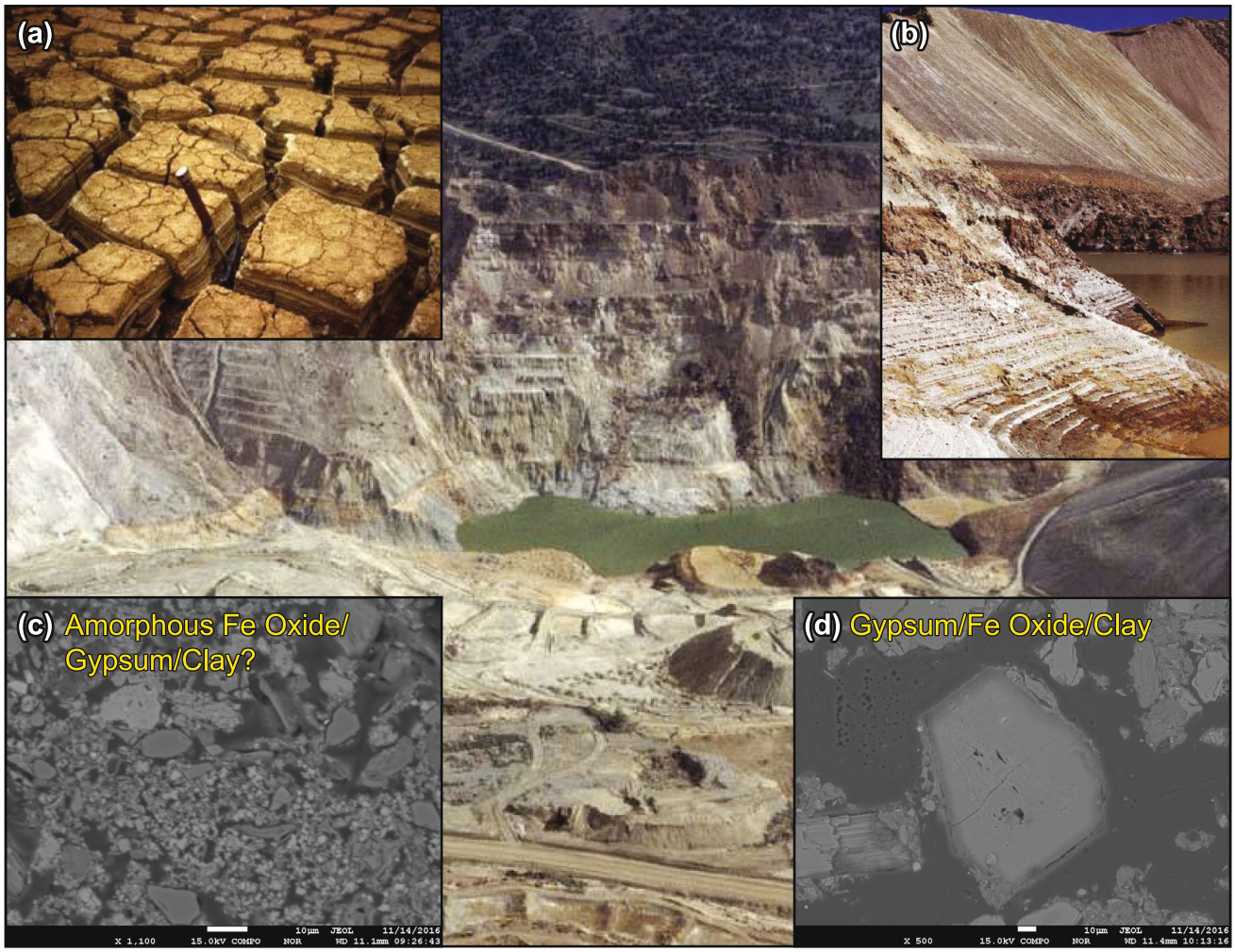

Fig. 2 The Liberty pit lake prior to its disappearance with, (**a**) varved amorphous ferric hydroxide, (**b**) gypsum precipitating on the pit lake shore, (**c**) precipitates corresponding to (**a**) and (**d**) precipitates corresponding to (**b**)

The phases in geochemical models generally represent solids with a crystalline structure and the log K_{sp} may differ for amorphous phases with the same chemical composition (Nordstrom 2020). The higher the log K_{sp}, the more soluble the compound. For example, for amorphous calcium carbonate, the log K_{sp} − 6.4 (Oral and Ercan 2018) is two orders of magnitude higher than that of crystalline calcite log K_{sp} − 8.48 (Oral and Ercan 2018), indicating that calcite is less prone to initial precipitation in solution. However, when considering basaluminite, the log K_{sp} value of 22.3 (Langmuir 1997; Younger et al. 2002) is comparable to that of amorphous basaluminite, which has a log K_{sp} of 24 (Nordstrom 2020).

While there are abundant theoretical and laboratory studies that provide extensive insight as to possible phases that may be expected to precipitate in acid and alkaline pit lakes, and there are many European pit lake precipitate studies, there is a dearth of information in the western USA where, of 87 mine sites in Nevada, 38 are or are expected to become pit lakes. While most will be < 10 ha, eight are expected to be more than 81 ha according to the NDEP (Rothberg 2023). Consequently, practical empirical observations on hard rock-hosted pit lake precipitates are necessary to provide insight on reasonable mineral assemblages to incorporate into pit lake studies in this setting.

This paper presents data collected over the course of four disparate studies, all in Nevada, USA, ranging from analysis of basal precipitates in the ephemeral Liberty acid pit lake and one in a limestone setting (the Cortez pit lake) where precipitates were collected and analyzed by XRD and EMPA, to precipitates collected during laboratory experiments titrating the formerly acid Lone Tree pit

lake water, culminating in the mineralogy of a precipitate profile in the now alkaline Lone Tree pit lake.

Materials and Methods

The Formerly Acidic Liberty Pit Lake

The Robinson porphyry copper district has been mined for over 100 years, resulting in three pits, Liberty, Tripp-Veteran, and Kimbley/Ruth. The ore at the Robinson mine is hosted in an intrusive monzonite porphyry surrounded by limestone, sandstone with intercalated limestone, shale, and rhyolite. Dewatering of the adjacent south block hydrogeologic unit resulted in segregation of a small acidic (pH 2.7) pond from the larger neutral pH pit lake and the eventual disappearance of both water bodies. In 1996, the pond contained 124 mg/L Fe, 610 mg/L Ca, 3370 mg/L SO_4, and a variety of metals and rare earths (Table 1).

The sediment/precipitates in the base of the pit were analyzed by EMPA following the method of Davis et al. (1992). Briefly, the sample was mounted in an epoxy mold, allowed to cure at room temperature, and polished at low speed using kerosene to prevent dissolution of water-soluble phases. The surface of the mold was then cleaned with isopropyl alcohol and coated with a thin layer of carbon to allow electrical conductance. Analysis was on a Joel 8600 microprobe operated at 15–20 kV, with IQ-20-nA specimen currents and a 1-µm-diameter beam.

Metal-bearing particles were identified using a combination of energy dispersive spectroscopy, wavelength dispersive spectroscopy, and backscatter electron image spectroscopy (BEI). Images of sediment particles were obtained using BEI and recorded as photomicrographs. The elemental composition of the material was established relative to EMPA standards to determine the stoichiometry of solid metal phases in the sample.

The Formerly Basic Cortez Pit Lake

The Cortez deposit is located on the alluvial floor of the east side of the Crescent Valley. Fine-grained disseminated gold is hosted primarily in the Devonian Wenban and Silurian Roberts Mountains units, which consist of dark grey, carbon-rich, calcareous to dolomitic siltstones that have been locally altered at the intersection of certain structural features.

The former shallow (≈ 8 m) Cortez pit lake began filling in 1973 after conclusion of mining, eventually draining between 1997 and 1999. The water quality was analyzed three times from 1992 through 1996 (Table 2) and was consistently alkaline (≈ 300 mg/L HCO_3), with pH 8.1–8.4, SO_4 (90 mg/L), and TDS (425–525 mg/L). Two samples of basal sediment were collected from the east and west side of the pit lake during evaporation (Fig. 3b). Sediment from the former Cortez pit lake was analyzed chemically and by EMPA to characterize the pit lake precipitates.

The Transitional Lone Tree Pit Lake

The Lone Tree mine is located in the western portion of the Pumpernickel Valley hydrographic basin in Humboldt County. There are four main geologic units in the pit consisting of: (1) quaternary alluvium, (2) sandstones, limestones, mudstones, and conglomerates, with some interbedded volcanic units of the Havallah Formation, (3) siltstones, sandstones, and arenite of the Edna Mountain Formation and conglomerate of the Battle Formation, and (4) the Valmy Formation, consisting mainly of quartzite and argillite.

The Lone Tree pit lake was acidic (pH 3.1) prior to treatment with lime (Table 3), with elevated Fe (≈ 30 mg/L), Al (≈ 48 mg/L), Mn (≈ 3.5 mg/L), and SO_4 (≈ 1785 mg/L). Arsenic was predominantly As^{5+} with non-detectable levels of As^{3+} (< 0.003 mg/L) in all samples. The ORP (≈ 500–530 mV) reflected oxidizing conditions with predominantly Fe^{3+}.

Initial efforts at pit lake neutralization began in 2008. The addition of ≈ 1306 tonnes of caustic soda [Na(OH)] occurred from August 2008 to March 2009; however, lake monitoring indicated only localized areas of alkalinity. Subsequently, a rotating cylinder treatment system (RCTS) plant to manufacture milk-of-lime slurry containing 3.5–17.5% lime was constructed and by August 2009 was in full production, producing ≈ 1.8 tonnes/day. Enhancement to the system in 2010 increased RCTS throughput to an average of ≈ 7.3 tonnes/day.

The pit lake chemistry did not show improvement at this lime treatment rate; therefore, a portable lime batching system was procured to accelerate production resulting by December 2010 in a circumneutral water column. In 2015, trona (sodium sesqui-carbonate) was selected as the sole source of alkalinity addition because its higher solubility enabled maximum dissolution rates in the surface water (Schafer et al. 2020). However, since 2018, the pH and alkalinity have steadily increased.

Titration Test

As part of pit lake mitigation, a bench-scale dosing study evaluated the geochemical response over a pH range of 4–8.8. The test measured the reduction in metal concentrations as the pit lake water was titrated with lime and

Table 1 Liberty pit lake water in 1996 with modeled precipitates

Parameter	NDEP Profile III Standard	Liberty pit 12/19/1996
Alkalinity	–	< 10
Chloride	–	50.7
Fluoride	2	12.6
Sulfate	–	3370
Mercury	0.01	0.0006
Aluminum	4.47	52
Barium	23.1	0.0024
Beryllium	2.83	0.0078
Cadmium	0.05	0.289
Calcium	–	610
Chromium	1	0.0199
Copper	0.5	47.8
Iron	–	124
Lithium	40.3	
Magnesium	–	287
Manganese	377	58.3
Molybdenum	0.6	1
Nickel	171	307
Phosphorus	–	< 5
Potassium	–	12.2
Sodium	2000	43.8
Strontium	1127	0.591
Tin	29.2	0.4
Vanadium	0.1	0.0026
Zinc	25	39.6
Antimony	0.29	0.0001
Arsenic	0.2	0.0118
Lead	0.1	0.0001
Selenium	0.05	< 0.0001
Thallium	0.032	0.005
NO_2/NO_3–N	100	0.15
pH	6.5–8.5	2.72

Modeled precipitates	SI**	Log IAP	Log K	
$CdMoO_4$	0.43	− 13.72	− 14.2	$CdMoO_4$
$CuMoO_4$	1.9	− 11.17	− 13.1	$CuMoO_4$
Cupricferrite	3.58	9.57	5.99	$CuFe_2O_4$
$Fe(OH)_{2.7}C_{1.3}$	5.06	2.02	− 3.04	$Fe(OH)_{2.7}C_{1.3}$
Ferrihydrite	0.58	3.77	3.19	$Fe(OH)_3$
Goethite	3.28	3.77	0.49	FeOOH
Gypsum	0.02	− 4.59	− 4.61	$CaSO_4{:}2H_2O$
H-Jarosite	7.54	− 4.56	− 12.1	$(H_3O)Fe_3(SO_4)_2(OH)_6$
$H_2Sn(OH)_6$	5.96	− 17.57	− 23.5	$H_2Sn(OH)_6$
Hematite	8.96	7.54	− 1.42	Fe_2O_3
K-Jarosite	9.51	− 5.29	− 14.8	$KFe_3(SO_4)_2(OH)_6$
Lepidocrocite	2.4	3.77	1.37	FeOOH
Maghemite	1.15	7.54	6.39	Fe_2O_3
Magnetite	0.34	3.74	3.4	Fe_3O_4
$MnHPO_4$	0.29	− 25.11	− 25.4	$MnHPO_4$

Table 1 (continued)

Modeled precipitates	SI**	Log IAP	Log K	
Na-Jarosite	6.7	− 4.5	− 11.2	$NaFe_3(SO_4)_2(OH)_6$
$NiMoO_4$	0.83	− 10.31	− 11.1	$NiMoO_4$
Nsutite	0.42	17.93	17.5	MnO_2
Pyrolusite	1.9	43.28	41.38	MnO_2
$Sn(OH)_4$	4.71	− 17.57	− 22.3	$Sn(OH)_4$
SnO_2	11.41	− 17.57	− 29	SnO_2
$SnSO_4$	9.48	− 47.49	− 57	$SnSO_4$
Strengite	2.97	− 23.43	− 26.4	$FePO_4{:}2H_2O$

Visual and microprobe evidence of occurrence

investigated the evolution of precipitating mineral phases as a function of pH.

Ten tests were run using the Lone Tree pit lake water titrated with a lime slurry to reach a final pH of ≈ 4, 5, 6, 7, and 8.8 (in duplicate). The time span of two continuous titrations to a final pH 8.8 was ≈ 8 h; however, no marked time dependency in the titration curves was apparent using shorter time intervals. During each test, a defined amount of lime was added at every step with continuous stirring. After adding the lime, the volume added, pH, and ORP were recorded, with mixing ceasing when the pH was stable within 0.1 units of the target. The samples were analyzed for major ions and metals, Si and P, for both unfiltered and filtered (0.45 µm) water. Colloids were deemed to have a minimal impact given the similar concentrations between filtered and total chemistry (Table 3). The precipitates formed during the tests were collected on the filters and analyzed by XRD and backscatter EMPA to determine the major phases.

Precipitate Trap Profiles

Precipitate traps were deployed on April 12, 2023, in two locations, at the shallower north end (N) where the trona slurry is added and at the deeper south end (S) of the pit lake (Fig. 4a). The traps consisted of a mason jar at each depth to which was attached a funnel with a 30 cm diameter mouth deployed at 8, 23, 46, and 76 m below lake surface (bls) in the north, and at 30 m intervals from 30 to 183 m bls in the south (Fig. 4b). When retrieved three months later (July 26), there was abundant amorphous floc in the jars (Fig. 4c).

The in-situ water column samples were air-dried and spiked with corundum to determine amorphous content, prepared for XRD analysis, and scanned over a range of 3° to 45° 2Θ Cu Kα radiation at 40 kV, 35 mA. Mineral phases were identified with the aid of computer-assisted programs accessing a powder diffraction database. Estimates of mineral concentrations were based on relative peak heights and measured reference intensity ratios. The north end floc from 38 and 76 m bls was also analyzed for total metals by SW-846 6010C (EPA 1996).

Geochemical Modeling

PHREEQC (Parkhurst and Appelo 1999) simulates aqueous chemical reactions based on equilibrium chemistry of an aqueous solution interacting with minerals, gases, solid solutions, exchangers, and sorption surfaces. PHREEQC version 3.3.5.10806, in conjunction with the modified MINTEQ.V4.DAT (Allison et al. 1998) thermodynamic database was used for speciation and the calculation of saturation indices (SI) from the Robinson 1996 (Table 1), Cortez 1996 (Table 2), and Lone Tree 2023 (Table 3) water chemistries. Based on Lydersen (1990), the solubility constant (log K_{sp}) for $Al(OH)_3$ decreases from 9.35 (for amorphous and microcrystalline phase precipitated within 2–20 weeks) to 7.97 (for well-crystallized gibbsite). Therefore, the log K_{sp} for amorphous $Al(OH)_3$ was set to 9.35 in the modified MINTEQ.V4.DAT version. In addition, $FeOHSO_4$ (log $K_{sp} = -10$) and schwertmannite (log $K_{sp} = 10.5$) were added to the database.

Table 2 Former Cortez pit lake analytical water chemistry data (mg/L)

Analyte	NDEP Profile III Standard	Geomega 10/9/1996	Bird et al 6/30/1993	West end 6/15/1992
Alkalinity	–	314	282	225
Aluminum	4.47	0.016	< 0.02	NA
Antimony	0.29	0.006	NA	NA
Arsenic	0.2	0.034	0.038	0.04
Barium	23.1	0.062	0.06	0.06
Cadmium	0.05	< 0.001	NA	< 0.007
Calcium	–	42	45	43
Chloride	–	24	24	27
Chromium	1	0.015	NA	< 0.01
Fluoride	2	1.42	2.4	1.76
Iron	–	< 0.01	0.134	< 0.05
Lead	0.1	0.002	0.0043	0.007
Magnesium	–	17	18	18
Manganese	377	< 0.005	0.0017	< 0.003
Mercury	0.01	< 0.0002	0.00046	0.0138
Nickel	171	0.006	NA	NA
Nitrate	100	< 0.05	0.21	< 1.0
pH (su)[a]	6.5–8.5	8.41	8.07	
Potassium	–	9	12	11
Selenium	0.05	< 0.001	NA	< 0.005
Silver	–	< 0.0005	NA	NA
Sodium	2000	64	69	71
Sulfate	–	91	90	82
Thallium	0.032	< 0.001	NA	NA
Total dissolved solids	7000	525	432	425
Zinc	25	0.002	0.002	0.006

Equilibrium phases	Present?	SI[c]
Log pCO_2	n.a	− 2.93
Calcite	Figure 2d	+ 0.99
Gypsum	x	− 1.62
AFH[b]	Table 3	+ 1.34
Barite	Figure 2d	+ 0.21
Fluorite	x	− 0.98
Dolomite	x	+ 1.87

[a]Standard units

[b]AFH = amorphous ferric hydroxide

[c]SI (Saturation Index) calculated by PHREEQC using non-detects at full value, 25 °C, and pe = 10

n.a not applicable

Results

Liberty Pit Sediment Mineralogy

The precipitates were visually different to the high wall rock with copious gypsum apparent on the bench just above the pit lake (Fig. 2b), while AFH with desiccation cracks exposed alternating gray and ochre clay-size (seasonal) varves as the pit lake dried up, demonstrating the accumulation of authigenic precipitates at the base of the pit (Fig. 2a). Microprobe analysis identified AFH and gypsum assemblages with possible clay (Fig. 2c) and a gypsum and Fe oxide rhomb (Fig. 2d). This mineralogy was consistent with the aqueous chemistry (Ca = 500 mg/L,

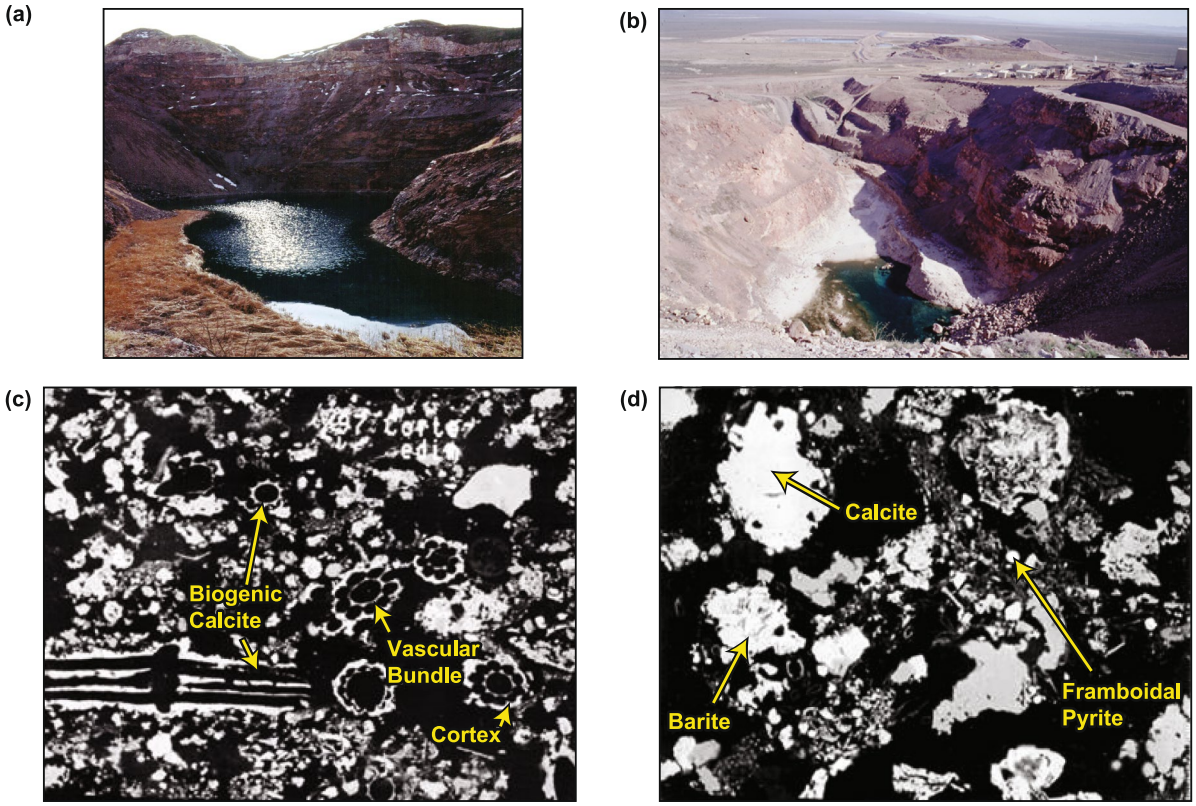

Fig. 3 (**a**) The former Cortez pit lake, (**b**) carbonate sediment showing as the pit lake diminished in size, (**c**) organic calcite replacing horsetail in longitudinal and cross section, and (**d**) the inorganic precipitate assemble

SO_4 = 3800 mg/L, Fe = 130 mg/L) that would have supported precipitation of gypsum at ≈ 400 mg/L Ca and 1000 mg/L SO_4 (based on equilibrium at an ionic strength of 0.0339; Drever 1982) and AFH.

Cortez Pit Lake Sediment Mineralogy

This sediment was also visually distinct from the pit wall material (Fig. 3b). The authigenic phases consisted predominantly of calcium carbonate, containing lesser quantities (0.1–1%) of Al, K, Fe, P, and SO_4, and trace amounts (0.01–0.1%) of Ba, Na, Mn, and Sr (Table 4). EMPA identified biogenic calcite replacing the solid portions, specifically the cortex and vascular bundles of horsetail stems (Fig. 3c), growing in and around the pit lake. Inorganic calcite and pyrite framboids (Fig. 3d) were also found, the latter consistent with the in situ microbially mediated precipitation of Fe sulfide noted in sediments elsewhere (Berner 1971; Davis et al. 1996).

Quantitative analysis of particles containing heavier elements demonstrated that barite and iron precipitates (Fig. 3d) were common authigenic phases (Table 4). Calcium carbonate sediment contained up to 200 mg/kg Ba, Mg (8800 mg/L), Mn (280 mg/L), and Zn (450 mg/L). Non-biogenic calcite contained up to 35 mg/kg Cd. The biogenic calcite contained trace amounts of Mg (up to 0.42%), Mn (0.012%), and Zn (0.023%), resulting in a solid solution phase of $Ca_{(0.995)}Mg_{(0.0042)}Mn_{(0.00012)}Zn_{(0.00023)}CO_3$.

Lone Tree

Basal Sediment Mineralogy

Contrary to the Liberty and Cortez pit lakes, visual verification was not possible for these pit lake sediments. However, in 2009, a SEM mineral liberation analysis reported that 94% was Fe-dominated clay, and this was confirmed by XRD.

Water Column Precipitate Traps

In 2023, an amorphous precipitate dominated the sediment composition at the north end, increasing from 51 to 78% through the depth of the profile at 76 m bls (Table 5). Calcite showed a consistent decrease from 8 to 76 m bls, by which depth it had dissolved. An XRD scan of trona used at Lone Tree found 92% trona ($Na_2CO_3 \cdot NaHCO_3 \cdot 2H_2O$) and evidence of calcite (< 2%), with dolomite (5%) and 1% quartz. The presence of calcite in trona explains its occurrence in

Table 3 Lone Tree average pit lake chemistry used in the titration experiments (2010) and in 2023 showing the contrast over 13 years of treatment

Parameters	NDEP profile III reference value	2010 Pit Lake Chemistry[a]		2023 Pit Lake Chemistry[b]	
		Unfiltered	Filtered	Unfiltered	Filtered
Alkalinity	–			78.6	78.6
Acidity, $CaCO_3$	–	469	479		
Aluminum	4.47	50	48.1	0.1	0.1
Antimony	0.29	0.03	0.02	0.047	0.049
Arsenic	0.2	0.21	0.11	0.02	0.04
Arsenic (III)		0.003	0.003	n.a	n.a
Arsenic (V)		0.21	0.11	n.a	n.a
Barium	23.1	0.05	0.05	0.04	0.04
Beryllium	2.83	0.02	0.01	0.002	0.002
Boron	5	0.89	0.89	n.a	0.86
Cadmium	0.05	0.10	0.10	0.002	0.002
Calcium	–	302	307	392	401
Chloride	–	19.1	22.1	21.4	21.4
Chromium	1	0.029	0.028	0.01	0.01
Copper	0.5	1.28	1.18	0.08	0.08
Fluoride	2	7.80	9.81	1.2	1.2
Iron	–	31.2	30	0.2	0.4
Iron (II)		4.7	n.a	n.a	n.a
Iron (III)		25.3	n.a	n.a	n.a
Lead	0.1	0.19	0.19	0.01	0.01
Magnesium	–	71.7	71.6	70.2	81.2
Manganese	377	3.52	3.53	0.48	0.49
Mercury	0.01	0.0002	0.0002	0.0005	0.0005
Nickel	171	1.96	1.86	0.01	0.14
Nitrite/nitrate, N	100	0.07	0.08	0.62	0.62
pH (su)	6.5–8.5	3.14	3.14	7.72	7.72
Phosphorus	–	0.14	0.09	0.05	1
Potassium	–	33.2	31.5	33	33
Selenium	0.05	0.0042	0.0039	0.01	0.01
Silicon	–	30	30	n.a	n.a
Silver	–	0.005	0.005	0.01	0.1
Sodium	2000	157	150	240	242
Sulfate	–	1695	1785	1600	1600
Thallium	0.032	0.044	0.042	0.001	0.001
Total dissolved solids	7000	2555	2598	2333	2333
Zinc	25	11.4	12.3	0.28	0.30

All units in mg/L, except pH in standard unit

n.a. not analyzed

[a]Average of four sampling dates from May 17 to 20, 2010

[b]Average of three sampling dates from January 24, February 20 to March 28, 2023

the north pit profile, while the absence of calcite in the south profile attests to trona's solubility in the pit lake.

Since there is no basis on which quartz should precipitate, it is probably due to highwall rock spall and/or from trona and was at a consistently low proportion (3–4%) to 76 m bls at the north end. Smectite was present in the entire north profile (5–16%) and at 183 m bls (21%) in the south profile. The presence of gold in this region is linked to sericitic and argillic alterations of siliciclastic rocks and dikes, as well as decarbonatization and alteration of carbonate-bearing units into Fe-carbonate, along with sulfide formations containing Fe-As, and fine-grained quartz alterations across all types of rocks. The argillic alteration encompasses various clay minerals such as kaolinite, smectite, and illite, suggesting

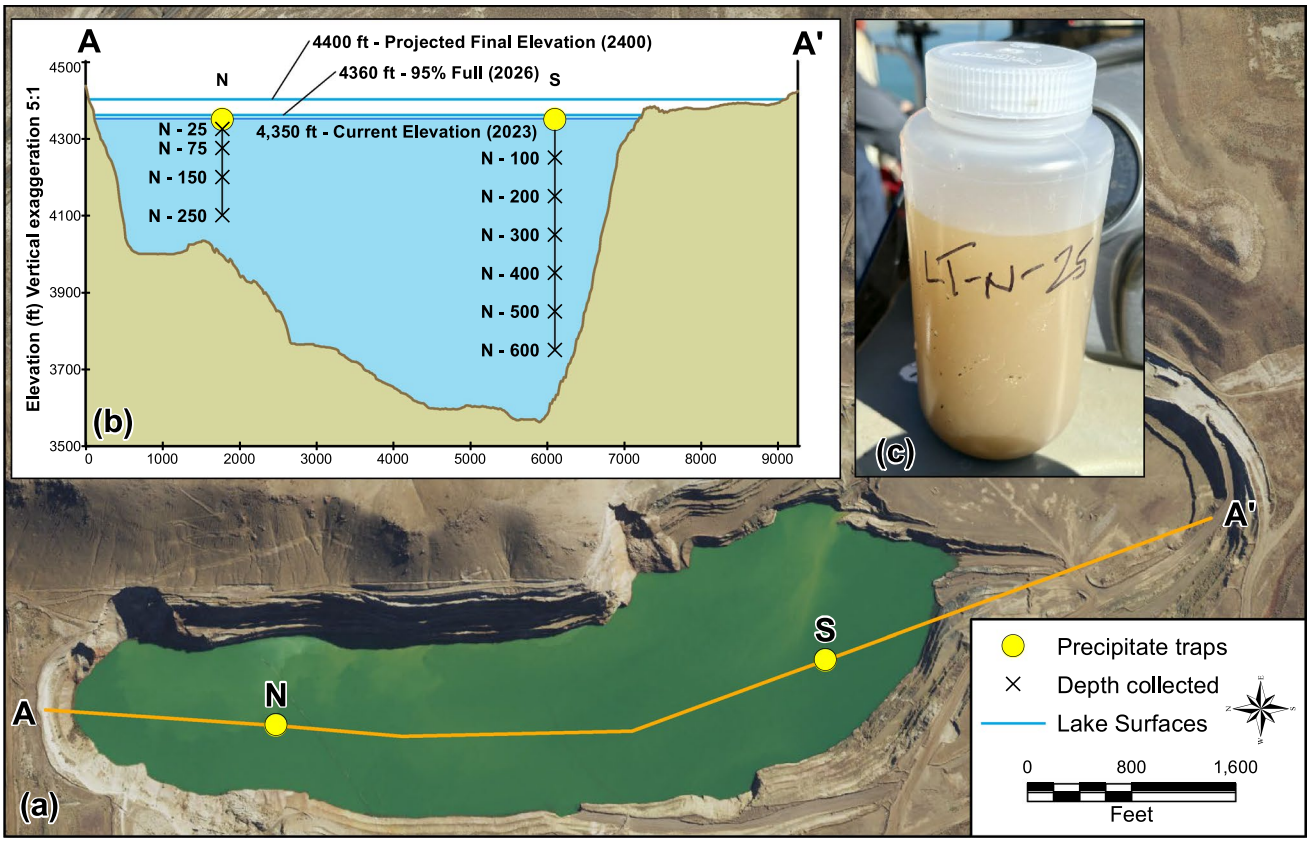

Fig. 4 (**a**) Locations of the precipitate traps, (**b**) disposition of the precipitate traps at locations N and S on (**a**), and (**c**) precipitate collected from N-25

that smectite may have originated from the surrounding wall rocks as detrital material (Holey et al. 2019).

The bulk metal concentrations for the precipitate subjacent to the north end trona application point at 46 m bls (Table S-1) included Fe (14.8%), Ca (29%), and Al (3.2%), with co-precipitated/sorbed As (0.6%), Cu (0.1%), Mn (0.75%), and Zn (0.27%).

In distinct contrast to the north end, south end precipitates were largely (≥96%) amorphous (Table 5) with minor quartz (3–4%) and trace amounts of calcite and K-feldspar at depth, the latter probably due to spall off the adjacent submerged highwall (Fig. 4b).

Titration Tests

The starting fluid was acidic (pH 3.1); consequently, dissolved Fe (30 mg/L) was similar to the total (31.2 mg/L with 4.7 mg/L Fe^{2+} and 25.3 mg/L Fe^{3}; Table 3). Sulfate was ≈ 1700 mg/L, and Al (50 mg/L), 300 times the Nevada Profile III ecological risk reference values. Using this water, two complete titration curves to a final pH of 8.8 were highly congruent (Fig. 5) with the complexity of the buffering system apparent from a comparison with titration of carbonic acid.

At pH 4, ≈ 30% of the Fe had precipitated (Fig. 6a), while above pH 4, Al was removed from solution (Fig. 6b), consistent with the EMPA precipitate formation. While these titration curves were similar to those obtained by Sánchez-España et al. (2011) for the San Telmo and Cueva de la Mora acidic pit lakes in Spain, although the carbonate buffering above pH 5.6 for Lone Tree appears more pronounced than for the Spanish pit lakes, their Fe^{3+}/schwertmannite and Al^{3+}/hydrobasaluminite buffer points were sharper than at Lone Tree. However, the Cueva de la Mora acid pit lakes contain Fe and Al concentrations five and three times greater, respectively, compared to the Lone Tree pit lake, possibly accounting for the sharper buffer points.

The titration curve between pH 3.1–4.5 was dominated by Fe buffering as dissolved Fe in the acidic water was oxidized, hydrolyzed, and precipitated, associated with the release of hydrogen ion due to the formation of AFH or Fe-oxyhydroxysulfate (schwertmannite), i.e.:

$$Fe^{2+} + 0.25O_2 + 2.5H_2O \rightarrow Fe(OH)_3 + 2H^+ \quad (1)$$

Table 4 Concentrations of trace metals in the Cortez pit lake sediment

Sr	Ba	Zn	Mg	Mn	Cd
Sample CP-1 collected from the north end of the pit					
0	200	0	8800	0	0
0	0	0	3300	60	0
0	0	0	4100	0	0
0	0	20	5300	0	0
Average concentration					
0	50	5	5375	15	0
Sample CP-2 collected from the west end of the pit					
0	70	400	4800	170	130
600	0	450	8800	0	50
0	0	0	4100	40	0
0	10	300	2400	280	380
0	0	0	2800	110	0
Average concentration					
120	16	230	4148	120	112

	Particle #	%
Particle distribution mineralogy of the heavy fraction Total particles counted = 215		
Pyrite	16	7
Zircon	15	7
Phosphate	11	5
Ilmenite	26	12
Fe oxide	22	10
Barite	71	33
Titanomagnetite	51	24
Rutile	3	1

Table 5 Lone Tree pit lake sediment mineralogy

	N-8	N-23	N-46	N-76
Amorphous	51	64	78	78
Calcite	39	14	5	–
Dolomite	1	4	2	3
Illite	–	5	5	–
Quartz	4	4	3	3
Smectite	5	9	7	16

	S-31	S-61	S-91	S-122	S-152	S-183
Amorphous	96	96	97	97	96	63
Quartz	4	4	3	3	4	9
Smectite	< 2	< 2	< 2	< 2	< 2	21
Calcite	–	–	–	–	–	2
K-Feldspar	–	–	–	–	–	5

$$8Fe^{3+} + 1.44SO_4^{2-} + 13.12H_2O \rightarrow Fe_8O_8(OH)_{5.12}\left(SO_4\right)_{1.44} + 21.12H^+ \quad (2)$$

Between pH 4.5 to 5.4, a second plateau occurred associated with Al buffering (basaluminite), i.e.:

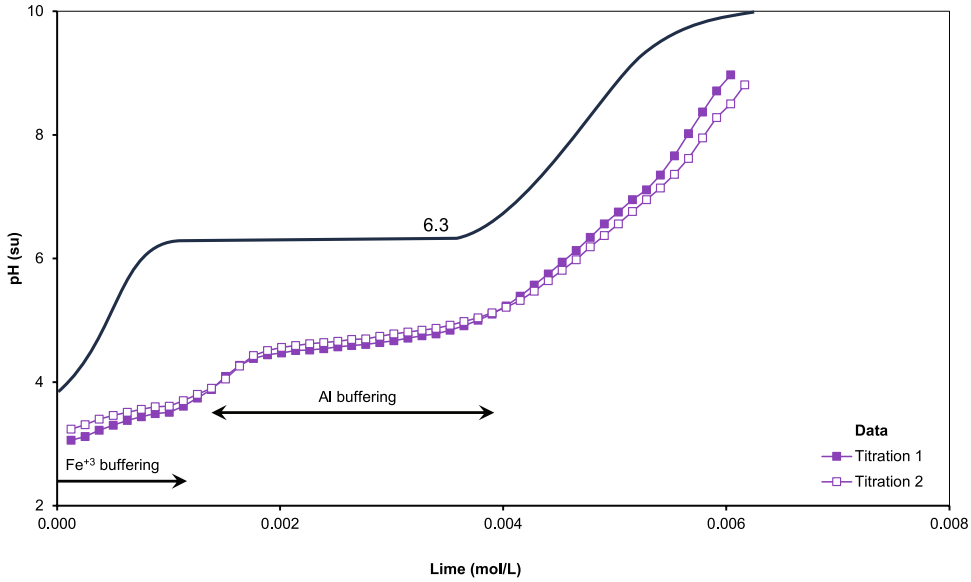

Fig. 5 The Lone Tree titration curves compared to the carbonic acid titration curve as base is added

$$Al^{3+} + 0.25SO_4^{2-} + 2.5_2O \rightarrow Al(OH)_{2.5}(SO_4)_{0.25} + 2.5H^+ \quad (3)$$

Starting at pH 5.5, the pH increased linearly, concurrent with precipitation of $Al(OH)_3$:

$$Al^{3+} + 3H_2O \rightarrow Al(OH)_3 + 3H^+ \quad (4)$$

Manganese started to decrease in solution by pH 7, but was only removed substantially (≈ 50%) from solution between 7 and 8.8 (Fig. 6c), i.e.:

$$Mn^{3+} + 2H_2O \rightarrow MnOOH + 3H^+ \quad (5)$$

Sánchez-España and Yusta (2019) noted that while Mn was initially present as Mn^{2+} in their test, that it underwent partial abiotic oxidation during titration, leading to the formation of mixed-valence Mn^{3+}/Mn^{4+} oxides/hydroxides.

Arsenic (Fig. 6d) and Sb (Fig. 6e) initially decreased at, and above pH 4, potentially co-precipitated with (Waychunas et al. 1993), or absorbed to AFH. Chromium was non-detect above pH 4 (Fig. 6f), while Pb (Fig. 6g) and Cu (Fig. 6h) decreased at pH 5 and above. Zinc (Fig. 6i), Cd (Fig. 6j), and Se (Fig. 6k) were removed from solution at pH 7 and above. Sulfate was non-reactive (Fig. 6l), as were Ba, B, Cl, K, and Tl in solution at any pH (Tables S-2 to S-11).

Discussion

The nexus between the precipitate chemistry and modeling was investigated for the Liberty and Cortez pit lake sediments (recognized as true aqueous precipitates due to their disparity from the adjacent wall rock). PHREEQC was also used to investigate the saturated mineral phases at pH 4 through 8.8 for the Lone Tree titration and for the 2023 pit lake chemistry. The objective of modeling the pit lake chemistry was to determine if their solution chemistries were consistent with the controls inferred from the precipitate mineralogy and if not, to determine the reasons behind the disparities.

Liberty Pit Lake

The precipitate consortium resulting from modeling the pit lake solution highlights the problem with indiscriminate selection of precipitates based solely on model results. For example, while only gypsum (SI + 0.02) and FeOOH (possibly aged to goethite) were diagnostically present in the theoretical mineralogic assemblage (Fig. 2c,d), the model identified 20 additional solids that could potentially precipitate from solution (Table 1).

Despite a high SI of 3.28, indicating strong supersaturation, goethite typically does not directly precipitate in Fe(III)-rich acidic pit lakes. It often forms as a transformation product of metastable precursors from AFH, ferrihydrite, or schwertmannite during early sediment diagenesis (Regenspurg et al. 2004; Sánchez-España et al. 2020) because it has slow precipitation kinetics and possibly a high activation energy for nucleation and crystal growth that impede its direct formation (Hamzaoui et al. 2002). While the PHREEQC model predicted many phases with a positive SI, most are unlikely to form due to kinetic constraints; therefore, in the absence of site-specific data to support their inclusion, there is no basis to infer their presence in a pit lake model.

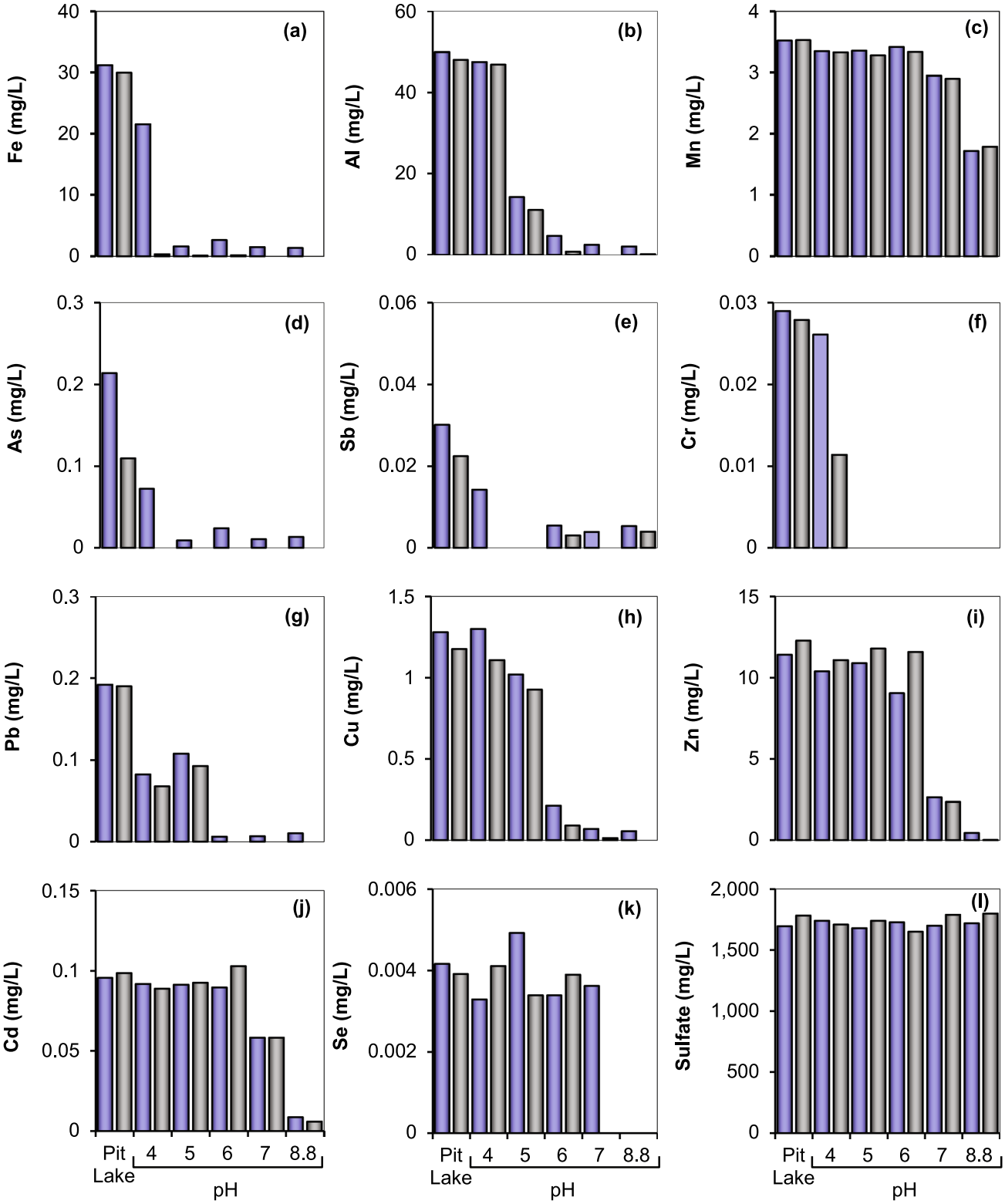

Fig. 6 Lime neutralization experimental results showing total (left) and dissolved (right) chemistry for duplicate analyses at each pH

Cortez Pit Lake

The biogenic calcite in the Cortez pit lake contained trace amounts of Mg (0.42%), Mn (0.012%), and Zn (0.023%) at the west end of the pit (Table 4), resulting in a solid solution phase of $Ca_{(0.995)}Mg_{(0.0042)}Mn_{(0.00012)}Zn_{(0.00023)}CO_3$. The resulting K_{sp} was incorporated into the PHREEQC database by defining a site-specific calcite phase using proportional representation of the calcite, magnesite ($MgCO_3$), rhodochrosite (Swallow et al. 1980; $MnCO_3$), and smithsonite ($ZnCO_3$) end member log K_{sp} values. However, the log K_{sp} for this phase was sufficiently similar to calcite (due to the similarity between the thermodynamic constants for the four carbonate phases), and because it consists of 99.5% calcite. Therefore, solid solution only affects trace metal chemistry (not Ca) concentrations. The presence of framboidal pyrite cannot be attributed to precipitation in the water column, but rather to in situ precipitation in the sediment because the pit lake was a shallow (≈ 8 m deep), well-oxygenated water body.

Precipitation of calcite is contingent on the pCO_2 of the system being modeled, particularly at neutral to alkaline pH values, which can be elevated due to CO_2 production from various sources including microbial degradation of organic matter, precipitation of calcite, and deep biological and thermogenic (e.g. magmatic) sources. Despite elevated pCO_2, calcite does not precipitate at low pH (< 4.5). Consequently, lakes may receive groundwater with pCO_2 as high as $10^{-1.7}$ atm (Cole et al. 1994; Langmuir 1971; Plummer and Wigley 1976). While the atmospheric pCO_2 is $10^{-3.5}$ atm (Berner and Berner 1996), in a survey of 1835 lakes worldwide, Cole et al. (1994) demonstrated that the global mean pCO_2 in lake surface waters is $10^{-2.98}$ atm, ≈ 3 times the atmospheric CO_2. The calculated pCO_2 was $10^{-2.93}$ atm in the Cortez pit lake (Table 2), typical of the supersaturated condition in other lakes.

The solid phases predicted to have SI > 0 (indicative of the propensity for that solid to precipitate) included calcite (+ 0.99), AFH (+ 1.34), barite (+ 0.21), and dolomite (+ 1.9). The results of geochemical modeling, the pit lake sediment chemistry (Table S-12), and the Cortez pit lake sediment mineralogy all support the hypothesis that incorporating barite, AFH, and calcite with a solid solution of selected cations is reasonable when modeling pH neutral to alkaline, limestone-hosted pit lakes.

Manganese in the Cortez pit lake was below detectable limits during the 1992 and 1996 measurements (Table 2), with negligible rhodochrosite present in the highwall (Fig. 3b), in distinct contrast to the Reochin pit lake, Cantabria, Spain, which contained elevated Mn (Sánchez-España and Yusta 2019). In the batch neutralization experiments using several IPB acidic pit lake waters (pH 2.7–4.2) with elevated Mn (358–892 mg/L) and trace metals (e.g. 0.8–10.4 mg/L Ni; 0.7–11 mg/L Co; 0.3–0.6 mg/L Zn), XRD and SEM analysis demonstrated Mn(III) as manganite [$Mn^{3+}O(OH)$], desautelsite [$Mg_6Mn^{3+}{}_2(CO_3)(OH)_{16}.4H_2O$], Mn(III/IV) as birnessite [$(Na, Ca, K)_x(Mn^{4+}Mn^{3+})_{2-x}O_4.1.5H_2O$) and todorokite [$(Na, Ca, K)_2(Mn^{4+}Mn^{3+})_6O_{12}.3–4{\cdot}5H_2O$] to Mn(IV) as asbolane [$Ni_{0.3}Co_{0.1}Ca_{0.1}Mn^{4+}{}_{1.5}O_{1.5}(OH)_2{\cdot}0.6(H_2O)$] at a final pH of 8.5–9 (Sánchez-España and Yusta 2019). Birnessite adsorbed trace metals (e.g. 1,424 mg/kg Co, 814 mg/kg Ni, and 2,713 mg/kg Zn), whereas asbolane contained Ni and Co.

Lone Tree

X-ray diffraction analysis identified amorphous precipitates across all pH. Based on their affiliated spectra, amorphous Fe- and Al-oxyhydroxysulfate were assumed to be the primary phases resulting from lime neutralization at pH 4 (Supplemental Fig. S-1), pH 5 (Supplemental Fig. S-2), and pH 6 (Supplemental Fig. S-3), with traces of AFH at pH 5. Aluminum hydroxide with Fe in the matrix (based on the spectra) was the primary phase at pH 7 (Supplemental Fig. S-4) and 8.8 where there were traces of $CaCO_3$, Zn affiliated with $Al(OH)_3$, barite, gypsum, and SiO_2, with the latter possibly a remnant particle from the original pit lake water (Supplemental Fig. S-5). Zinc appeared for the first time in the pH 7 spectra. Based on the geochemical model, while zincite (ZnO) was undersaturated (SI − 1.6), willemite (Zn_2SiO_4) was supersaturated (SI + 0.47). Willemite typically forms during low-temperature alteration of ZnS in arid environments, e.g. Goodsprings, Nevada (Takahashi 1960), and Broken Hill in Rhodesia (Brugger et al. 2003). Additionally, this mineral remains stable under oxidizing conditions at pH > 6 (Brugger et al. 2003).

Aluminum mineralogy evolved as the pH increased, with EMPA phases in alignment with the theoretical calculations of Lindsay and Walthall (1995) who demonstrated that alunite would be the stable phase below pH ≈ 5.5, above which gibbsite predominated, while Nordstrom and Nicholson (2017) described a white aluminous precipitate approximating basaluminite at a caved-in mine portal in Colorado.

However, using the a_K ($10^{-3.1}$) and a_{SO4} ($10^{-1.7}$) data with the solubility data from Nordstrom (1982) failed to identify any particular Al solubility-controlling phase (Fig. 7), possibly because for both the titration and the pit lake chemistry, Al solubility was controlled by coprecipitation with Fe-oxyhydroxysulfate. This hypothesis is supported by both the Fe concentration trends (decreasing) with increasing pH and by the photomicrographs that identified a mixture of $AlSO_4$ and $FeSO_4$ at pH 5 (Fig. S-2) and 6 (Fig. S-3).

Superimposing the pH/ORP neutralization path on a Fe/Mn Eh–pH diagram (Fig. 8) at pH 4 and pH 8.8 show little difference in locations of the aqueous/solid phase

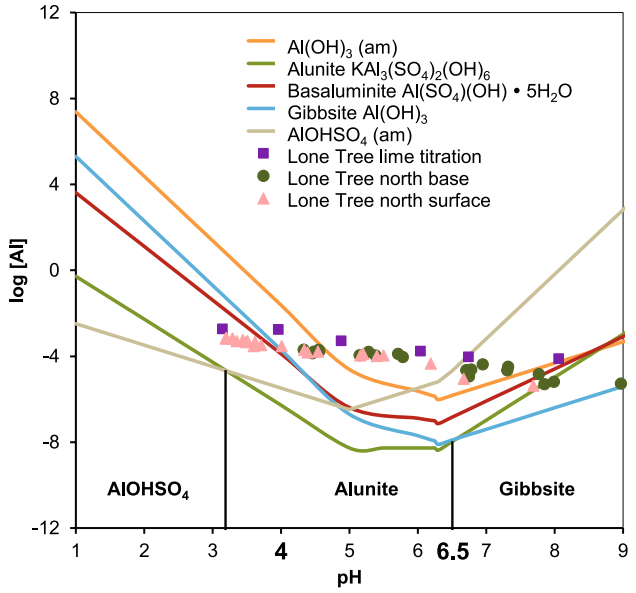

Fig. 7 Solubility curves for alunite, basalumite, gibbsite, and $AlOHSO_4$ (am) for a K activity of $10^{-3.1}$ and a SO_4 of $10^{-1.7}$ with the pH range of the stable phases identified

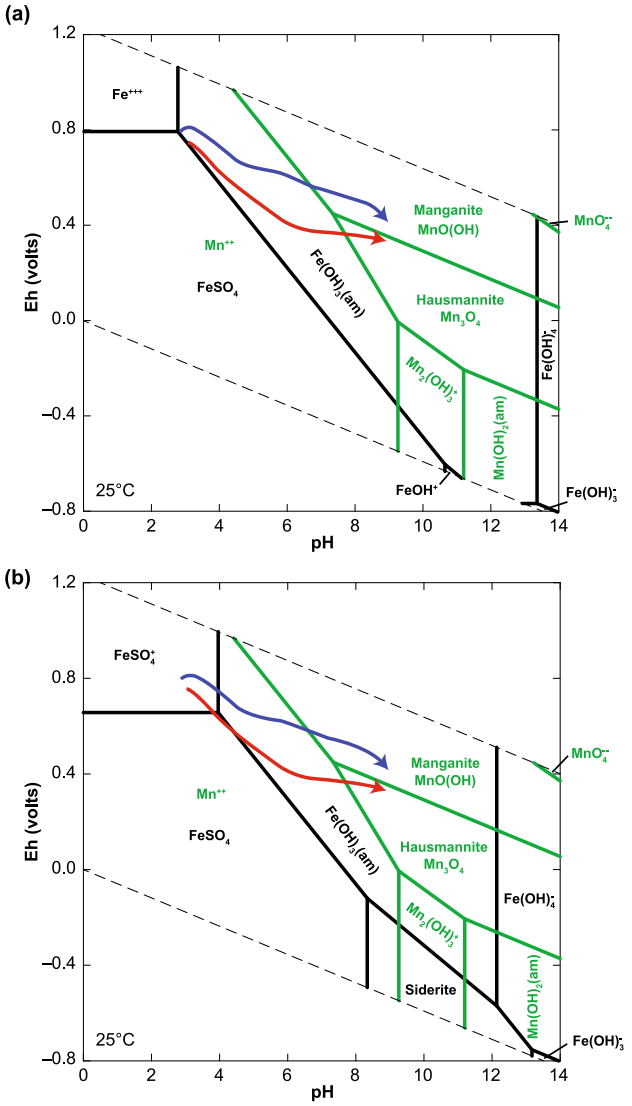

Fig. 8 Fe and Mn Eh-pH diagrams at (**a**) pH 4 (Fe = $10^{-3.25}$ mol/L), and (**b**) pH 8 (Fe = $10^{-4.6}$ mol/L). The blue and red lines show the path of the duplicate titrations in Eh-pH space

boundaries. Iron is in the $FeSO_{4(s)}$ zone under acidic conditions, possibly as a very fine-grained, amorphous material with a composition similar to a schwertmannite-type $[Fe^{+3}{}_{16}O_{16}(OH)_{12}(SO_4)_2]$ phase (Gaines et al. 1997). At pH 5, Fe precipitated in a mixed hydroxide/sulfate form until pH 7, when AFH predominated. Manganese, although not a notable peak in the pH 8.8 spectra (Fig. S-5), was ≈ 50% removed from solution by pH 8.8, consistent with the theoretical precipitation (Fig. 8) of either manganite [MnO(OH)] or hausmannite ($Mn^{2+}Mn^{3+}{}_2O_4$).

Kinniburgh et al. (1976) investigated a pH-dependent cation adsorption sequence to synthetic Fe hydroxide gel. Superimposing the Lone Tree titration data shows attenuation of Cr > Pb > Cu > Zn > Cd with Cd and Zn transposed from the Kinniburgh et al. (1976) order (Fig. 9). The approximate pH_{50} for Cr, Cu, Ni, and Zn were similar to the Kinniburgh pH_{50}, except for Cd with a pH_{50} ≈ 1 unit higher. These data support the proposition that the Lone Tree AFH was juvenile, because Kinniburgh's gel was freshly prepared in the laboratory.

Liming of the pit lake in 2014 resulted in a pH increase from 4.3 to 9 over a 5-month period, with a concomitant decrease in Cu, Zn, and Ni (Fig. 9) that was generally consistent with the Kinniburgh et al. (1976) curves, except that the Cu pH_{50} was ≈ 1 unit higher, while the Ni curve lacked hysteresis. Apart from AFH, amorphous Fe- and Al-oxyhydroxysulfate, Al oxyhydroxide, manganite, or hausmannite could also have potentially adsorbed or co-precipitated Cu, Cd, Cr, Ni, and Zn, as suggested by a decrease in Al and Mn with increasing pH, mirroring the Fe behavior. However, in this study, we were unable to differentiate between the processes of adsorption and coprecipitation of these metals.

Geochemical modeling of the titrated solutions indicated potential AFH and schwertmannite precipitation between pH 4–8.8, and amorphous Fe-oxyhydroxysulfate ($FeOHSO_4$) between pH 4–7 (Table 6). EMPA of titration precipitates (Figs. S-1, -2 and -3) identified Fe combined with S, suggesting amorphous $FeOHSO_4$ at pH 4–6. At pH 5, AFH containing Ca was also present. Gibbsite and amorphous $Al(OH)_3$ were undersaturated at pH 4 and 5, but supersaturated at pH 6–8.8, with the potential presence of amorphous Al-oxyhydroxysulfate ($AlOHSO_4$) at pH 5 and 6, corroborated by EMPA.

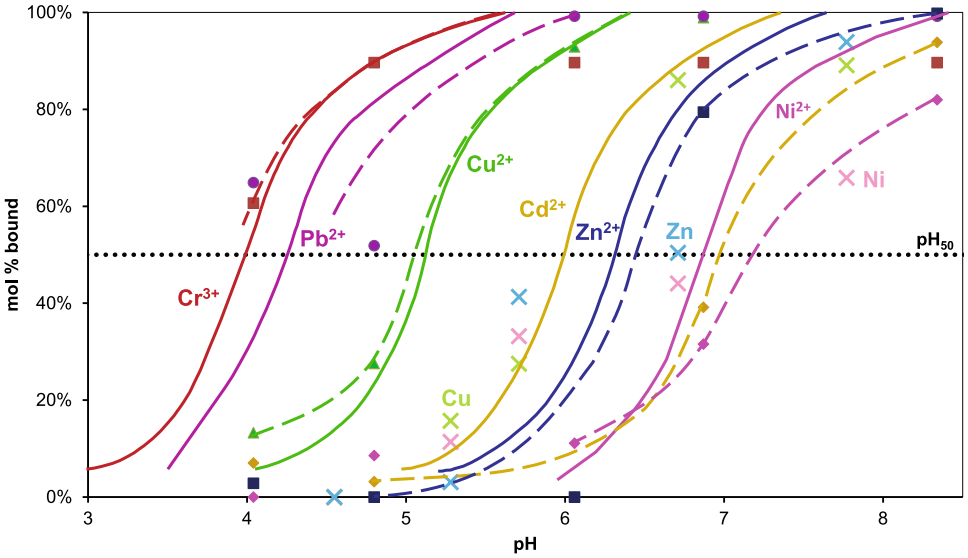

Fig. 9 Attenuation of trace metals in the titration experiment (— —) and in the Lone Tree pit lake in 2013 through 2014 between pH 4-8 compared to adsorption to fresh $Fe(OH)_3$ gel (Kinniburgh et al. 1976)

Table 6 Average Lone Tree saturation indices for relevant Al, Fe, and Mn phases for the two titrations

Phases	Composition	pH 4	pH 5	pH 6	pH 7	pH 8.8
Amorphous Al hydroxide	$Al(OH)_3$	–	–	2.3	2.19	1.4
Gibbsite	$Al(OH)_3$	–	–	3.36	3.25	2.46
Basaluminite	$Al_4(OH)_{10}SO_4$	–	–	9.51	7.05	2.6
Aluminum oxyhydroxysulfate	$AlOHSO_4$	–	0.1	0.47	–	–
Ferrihydrite	$Fe(OH)_3$	1.43	1.34	3.09	3.99	4.22
Ferric oxyhydroxysulfate	$FeOHSO_4$	5.17	3.19	1.87	0.75	–
Schwertmannite	$Fe_8O_8(OH)_6(SO_4)$	17.04	14.41	25.35	30.5	31.1
Manganite	MnOOH	–	–	2.64	4.58	5.61

As shown by the Eh–pH plots (Fig. 8), manganite (MnOOH) attained saturation at pH 6, increasing through pH 8.8. The model results were consistent with both the mineralogy, and with the sediment trap bulk metal chemistry (Supplemental Table S-1), in that the precipitate from 46 m bls was predominantly Ca (29%), presumably from the trona, Fe (15%) and Al (3%), with trace As (0.6%), Zn (0.3%) and Cu (0.1%).

The *Nexus* Between Pit Lake Chemistry, Precipitates, and Modeling

Between 2018 and 2023, there was a clear upward trend in the pit lake pH (Fig. 10a). Starting at pH 6.9 in January 2018, the pH increased steadily and reached ≈ 8 by February 2023, reflecting the corresponding rise in alkalinity from 33 mg/L $CaCO_3$ in January 2018 to 77 mg/L by February 2023. These observations, while demonstrating that trona is being added in excess, reflect its efficacy based on the progressive elevation of both pH and alkalinity levels with a decrease in SO_4 from ≈ 2000 mg/L to ≈ 1500 mg/L (Fig. 10e), presumably due to gypsum precipitation.

Other constituents showed the effect of increased pH (Fig. 10a), with differences in total and dissolved Al (Fig. 10b) and Fe (Fig. 10c) concentrations due to Al and Fe hydroxide precipitation (as demonstrated by the results of the titration test and the precipitate profile) that incorporated As (and other metals) within the AFH structure. For example, Cd (Fig. 10g) and Zn (Fig. 10h) decreased as the pH increased, consistent with Kinniburgh et al. 1976 (Fig. 9). Conversely, dissolved As (Fig. 10i) increased over the period, presumably due to desorption from AFH, which remained relatively stable through the period, while Mn (Fig. 10d) decreased sharply in 2022 when the pH exceeded 7, consistent with the precipitation of manganite (Fig. 8b).

Modeling the Contemporary Lone Tree Pit Lake

The pit lake chemistry from the north middle depth station in 2023 modeled using the dataset in Table 3 was consistent with the interpretations of the Eh–pH diagram at pH 7.7

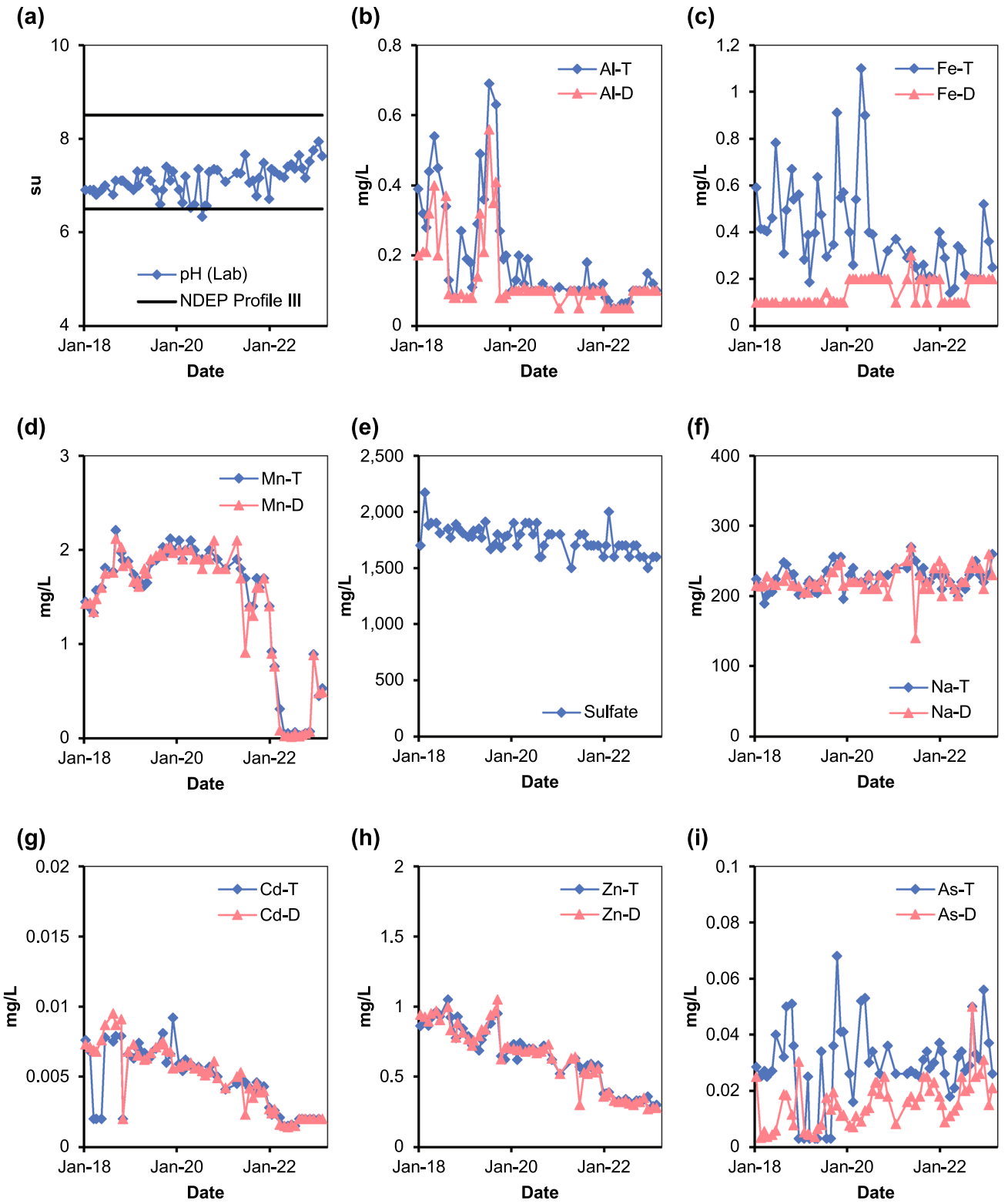

Fig. 10 A comparison of the total versus dissolved Lone Tree pit lake chemistry from 2018 to 2023

Table 7 Mineral precipitates identified in pit lakes

Location/deposit	Pit lake condition	Available information	Precipitates	Trace metals incorporated	Method	References
Berkeley Pit Lake, Montana, USA; copper porphyry	Acidic pit lake	Water column floc	Al Ca Fe (SO_4)	Cu, K, Mn, Zn	Suspended solids	Davis and Ashenburg (1989)
		1985 Visual observation	$FeSO_4$			
			$Fe(OH)_3$			
		Precipitates	Gypsum		XRD	Twidwell (2006)
			Jarosite			
Liberty, Ely, Nevada, USA; copper porphyry	Former acidic pond	Basal sediment	Amorphous $Fe(OH)_3$	Unknown	EMPA	Geomega (1997)
			Gypsum			
Lone Tree Pit Lake, Nevada, USA; gold mine	Acidic pit lake	2009 Basal sediment	Fe-Clay	As, Fe in clay	XRD/MLA	Geomega (2010)
			FeO			
Lone Tree Pit Lake, Nevada, USA; gold mine	Titration of acidic water	Precipitates	Amorphous $FeSO_4$		EMPA	Geomega (2010)
			Amorphous $AlSO_4$			
			$Fe(OH)_3$	Ca, Cr_3^+, Cd, Cu, Ni, Pb, Zn		
			$Al(OH)_3$			
			Barite			
			Gypsum			
			Trace carbonates			
Lone Tree Pit Lake, Nevada, USA; gold mine	Alkaline pit lake	Profile precipitates	amorphous Fe			Current study
			smectite			
Cortez Pit Lake, Nevada, USA; gold mine	Former alkaline pit lake	1996 Basal sediment	Calcite	Ba, Cd, Mg, Mn, Sr, Zn	EMPA	Geomega (2001)
			Barite			
			FeO			
San Telmo pit lake, Spain; lead	Acid pit lake	Profile precipitates	Schwertmannite		SEM, EDS, EMPA	Sanchez-Espana et al. (2012)
			Jarosite			Cánovas et al. (2012)
		Bottom sediment cores	Schwertmannite		XRD, SEM, FTIR	Cánovas et al. (2015)
			Jarosite			
			Barite			
			Anglesite			
			Goethite			
Cueva dela Mora, Spain; lead	Acid pit lake	Profile precipitates	Schwertmannite		SEM, EDS, EMPA	Sanchez-Espana et al. (2011)
			Jarosite			
			Goethite			
Cueva dela Mora, San Telmo, Spain; lead	Titration of acidic water	Precipitates	Schwertmannite		SEM, EDS, EMPA	Sanchez-Espana et al. (2011)
			Hydrobasaluminite			

Table 7 (continued)

Location/deposit	Pit lake condition	Available information	Precipitates	Trace metals incorporated	Method	References
San Telmo, Cueva de la Mora and Herrerias, Spain; copper, zinc, and lead	Acid pit lake	Suspended solid	Schwertmannite	Al, As, Pb	ICP, XRD, SEM, FESEM, TEM, HRTEM	Sanchez-Espana et al. (2016)
			Jarosite			
			Alunite			
Brunita Pit Lake, Spain; zinc and lead	Acid saline pit lake	Suspended solid	Jarosite (K, Na, and H_3O^+)		SEM	Sanchez-Espana et al. (2019)
			Schwertmannite			
			Goethite (aging)			
			ZnS associated with bacteria (amorphous to more crystalline over time)	Cd		
			PbS			
Lomnice and Jiri Pit Lake, Czechia; lignite mine	Acidic Pit Lake	Pit wall interface	Schwertmannite		XRD, IR, Mossbauer spectroscopy	Murad and Rojik (2005)
			Goethite			
			Jarosite			
Filón Centro, Tharsis Mine, Spain; Sulfur and copper	Acidic Pit Lake	Water column	Schwertmannite		SEM, TEM	van der Graaf et al. (2020)
			Jarosite			
			ZnS	As, Cd		
			CuS			
			Digenite ($Cu_{1.8}S$)			
			Djurleite ($Cu_{1.96}S$)			
			Chalcocite (Cu_2S)			
La Zarza, Spain; Sulfur and copper	Acidic Pit Lake	Water column	Schwertmannite		SEM, TEM	van der Graaf et al. (2020)
			Jarosite			
			ZnS			
			CuS			
Confesionarios Pit Lake, Spain; sulfide	Acidic Pit Lake	Bottom sediment core	Jarosite		XRD	Sanchez-Espana et al. (2009)
			Goethite			
Cueva de la Mora Pit Lake, Spain; lead	Acidic Pit Lake	Sediments from the lake shore and floating biofilms	Jarosite		XRD	Sanchez-Espana et al. (2005a, 2009; b)
			Schwertmannite			

Table 7 (continued)

Location/deposit	Pit lake condition	Available information	Precipitates	Trace metals incorporated	Method	References
			Goethite			
Cueva de la Mora Pit Lake, Spain; sulfide	Acidic Pit Lake	Water column	ZnS	Cu, Cd, Pb, As	SEM, TEM	Diez-Ercilla et al. (2014)
			CuS			
			As_2S_3			
		Sediment core	Schwertmannite		XRD, XRF, SEM	Diez-Ercilla et al. (2019)
			Jarosite			
			Amorphous Al precipitate (amorphous hydrobasaluminite)			
			Hydrobasaluminite			
			ZnS			
			PbS			
Cueva de la Mora Pit Lake, Spain; sulfide	Acidic Pit Lake	Sediment core	Detrital minerals: quartz, chlorite, muscovite, feldspar			Sanchez-Espana et al. (2005); Wendt-Potthoff et al. (2012)
		Water column	Jarosite		SEM	Sanchez-Espana et al. (2010)
			Schwertmannite			
Lusatian Pit Lakes (ML 111 Mine Plessa and ML 107 Mine Agnes), Germany; lignite mine	Acidic Pit Lake	Sediment core	Jarosite			Meier et al. (2004)
			Goethite			Gottlicher and Gasharova (2000)
			S			Pyzik and Sommer (1981)
			FeS, FeS_2			
Lausaitz (ML 77, ML 117, ML 107, ML 111, ML 13, ML F, Spreetal NO, Kortitzmuhle, Koschen, Bluno, Skado, Sedlitz), MittelDeutschland (Borna Ost, Niemegk), Oberpfalz (Murnersee, Bruckelsee, Ausee, Lindensee), Germany; lignite mines	Acidic Pit Lake	Water column	Schwertmannite		XRD, FTIR, SEM, extraction	Regenspurg et al. (2004)
		Sediment core	Jarosite			
			Goethite			

Table 7 (continued)

Location/deposit	Pit lake condition	Available information	Precipitates	Trace metals incorporated	Method	References
			Ferrihydrite			
			Gypsum			
Aerodrome and Twin Lakes, Western Australia; weathered igneous andmetamorphic rocks	Acid Saline Lake	Secondary precipitates	Micas		XRD, SEM	Story et al. (2010)
			Kaolinite			
			Dickite			
			Halloysite			
			Smectite			
			Chlorite			
			Alunite			
			Jarosite			
			Gypsum			
			Rozenite			
			Hydrobasaluminite			
			Hematite			
			Goethite			
			Anatase			
			Gibbsite			
			Mullite			
Medard Pit Lake, Czechia; lignite mine	Alkaline pit lake	Bottom sediment cores	Fe-oxyhydroxides (poorly crystalline)	As, V, REE (lanthanides)	XRD	Umbría-Salinas et al. (2021)
Medard Pit Lake, Czechia; lignite mine	Alkaline pit lake	Bottom sediment cores	Amorphous ferric hydroxide		XRD	Petrash et al. (2022)
			Nanocrystalline ferrihydrite			
			Mn(IV) oxyhydroxides			
			Siderite			
			Gypsum			
			Pyrite			
Harvard Pit Lake, California,USA; sulfide	Alkaline Pit Lake	Pit wall and joints containing efflorescent minerals	Goethite		XRD, XAS	Savage et al. (2009)
			Gypsum			
			Magnesiocopiapite			
			Jarosite			

Table 7 (continued)

Location/deposit	Pit lake condition	Available information	Precipitates	Trace metals incorporated	Method	References
			Epsomite			
			Fe oxyhydroxide (ferrihydrite)			
			Hexahydrite			
			Pentahydrite			
			Starkeyite			
			Rozenite			
			Halotrichite			
			Loeweite			
			Slavikite			
			Weilite			
Mono Lake, California, USA	Alkaline Pit Lake	Secondary precipitates	Ikaite		XRD	Council & Bennett (2015)
			Gaylussite			

(Fig. 8), confirming precipitation of AFH (SI = 3.9), manganite (SI = 5.9), and gibbsite (SI = 0.65) (Fig. S-4).

Conclusions

This analysis spans nearly four decades of investigations into pit lakes, beginning with visual observations and analysis of the Berkeley pit in 1985 and extending to the examination of precipitates in basal sediments, titration tests, and the installation of precipitate traps at Lone Tree in 2023. It includes summaries of findings from various pit lakes and lakes worldwide, including those in Spain (IPB), Germany (Lausitz, Mitteldeutschland, and Oberpfalz), the Czech Republic (Lomnice and Jiri), Western Australia (Aerodrome and Twin), Czechia (Medard), and California, USA (Harvard and Mono Lake).

Based on analyses of sediment and water column mineralogy in both acidic and alkaline pit lakes, as well as mineralogy observed in titration tests spanning a pH range from 4 to 8.8, a representative mineralogy for modeling pit lake chemogenesis emerges that includes a consistent set of solid phases from amorphous Fe- and Al-oxyhydroxysulfate/hydroxide to poorly crystalline jarosite, alunite, schwertmannite, and hydrobasaluminite, then to crystalline gypsum, barite, and clays in acidic lakes. In alkaline environments, calcite, ikaite, gaylaussite, siderite, AFH, gypsum, and barite with biogenic Fe oxyhydroxides and carbonates may be present with metal sulfides in basal pit lake sediment resulting from microbial activity in anoxic conditions (Table 7).

Adding to the complexity of pit lake precipitate mechanics is the kinetic rate of transformation of AFH to the more crystalline goethite and hematite. Schwertmann and Murad (1983) demonstrated that at 25 °C, goethite formed from AFH at pH 4 with a half-conversion period ($t_{½}$) of ≈ 250 days, while at pH 8, hematite was preferentially generated with a $t_{½}$ of ≈ 75 days. Sánchez-España et al. (2011) confirmed that goethite resulted from the aging of schwertmannite and jarosite, with Sánchez-España et al. (2012) concluding that metastable schwertmannite was converted to jarosite while descending through the water column. Consequently, the settling velocity of floc in the pit lake water column becomes a relevant consideration when considering phases to incorporate in a pit lake model.

The removal of solutes by AFH precipitation controls the solubility of Cd, Cu, Pb, and Zn at pH > 5 and As, Cr(VI), Mo, and Se at pH < 7.5. The precipitation and settling of AFH throughout the water column results in the sequestration of solutes from the solution, eventually forming a metal-rich sludge at the base of the pit. Besides AFH, other precipitates, e.g. schwertmannite, alunite,

hydrobasaluminite, various Al hydroxides, and carbonates can also sorb or coprecipitate metals.

Collecting relevant data depends on which of three possible pit lake scenarios require analysis, e.g. (1) if a pit lake has already formed, (2) if the pit lake is an expected outcome of an existing pit expansion, and (3) when permitting is undertaken to develop a new pit. For existing pit lakes, collection of empirical data to justify selection of precipitates may be obtained by installing precipitate traps through the pit lake profile, as at Lone Tree and other locations. In the event of a mine expansion, the chemical composition of surface water runoff collecting on benches, or in ponds forming at the base of the pit, may provide insight as to future pit lake conditions.

For pits in the permitting process, construction of an analog pit lake laboratory test using the high wall lithologic ratios, in conjunction with groundwater as the lixiviant, or mixing kinetic test leachates in the appropriate ratios may provide an opportunity to test assumptions regarding potential precipitates inherent in the model. Ultimately, the objective should be to shrink the error bars to improve model accuracy, so that mine management and regulators can make the best objective decisions related to environmental impacts for current and future pit lakes.

Supplementary Information The online version contains supplementary material available at https://doi.org/10.1007/s10230-024-00989-z.

Acknowledgements The authors appreciate the comments and suggestions of two anonymous reviewers on an earlier version of this manuscript that greatly improved the content.

References

Acero P, Hudson-Edwards KA (2022) Trace element uptake in fresh and aged aluminum oxyhydroxysulfates and hydroxides: implications for mine drainage-affected environments. Appl Geochem 146:105444–105451. https://doi.org/10.1016/j.apgeochem.2022.105444

Allison JD, Brown DS, Novo-Gradac KH (1998) MINTEQA2/PRODEFA2, A geochemical assessment model for environmental systems. U.S. Environmental Protection Agency Environmental Research Laboratory, Center for Exposure Assessment Modeling, Athens

Berner RA (1971) Principles of chemical sedimentology. The McGraw-Hill Inc, New York

Berner EK, Berner RA (1996) Global environment: water, air, and geochemical cycles. The Prentice Hall, Upper Saddle River

Bigham JM, Schwertmann U, Traina SJ, Winland RL, Wolf M (1996) Schwertmannite and the chemical modeling of iron in acid sulfate waters. Geochim Cosmochim Acta 60(12):2111–2121. https://doi.org/10.1016/0016-7037(96)00091-9

Bigham JM, Nordstrom DK (2000) Iron and aluminum hydroxysulfates from acid sulfate waters. In: Alpers CN, Jambor JL and Nordstrom DK (eds) Reviews in mineralogy and geochemistry, vol 40, Sulfate minerals—crystallography, geochemistry, and environmental significance, mineralogical Soc of America, Washington, D.C., pp 351–403. https://doi.org/10.2138/rmg.2000.40.7

van Breeman N (1976) Genesis and solution chemistry of acid sulfate soils in Thailand. PhD Diss, Agricul Res Report, vol 848–850

Brugger J, McPhail DC, Wallace M, Waters J (2003) Formation of willemite in hydrothermal environments. Econ Geol 98(4):819–835. https://doi.org/10.2113/gsecongeo.98.4.819

Cherniak DJ (1997) An experimental study of strontium and lead diffusion in calcite, and implications for carbonate diagenesis and metamorphism. Geochim Cosmochim Acta 61(19):4173–4179. https://doi.org/10.1016/S0016-7037(97)00236-6

Chiarello RP, Sturchio NC, Grace JD, Geissbuhler P, Sorensen LB, Cheng L, Xu S (1997) Otavite-calcite solid-solution formation at the calcite-water interface studied in situ by synchrotron X-ray scattering. Geochim Cosmochim Acta 61(7):1467–1474. https://doi.org/10.1016/S0016-7037(97)00010-0

Cole JJ, Caraco NF, Kling GW, Kratz TK (1994) Carbon dioxide supersaturation in the surface waters of lakes. Science 265(5178):1568–1570. https://doi.org/10.1126/science.265.5178.1568

Council TC, Bennett PC (2015) Geochemistry of ikaite formation at Mono Lake, California: implication for the origin of tufa mounds. Geology 21(11):971–974. https://doi.org/10.1130/0091-7613(1993)021%3c0971:GOIFAM%3e2.3.CO;2

Davis A, Ashenberg D (1989) The aqueous geochemistry of the Berkeley Pit, Butte, Montana, USA. Appl Geochem 4(1):23–36. https://doi.org/10.1016/0883-2927(89)90056-5

Davis JA, Fuller CC, Cook AD (1987) A model for trace metal sorption processes at the calcite surface: adsorption of Cd^{2+} and subsequent solid solution formation. Geochim Cosmochim Acta 51(6):1477–1490. https://doi.org/10.1016/0016-7037(87)90330-9

Davis A, Ruby MV, Bergstrom PD (1992) Bioavailability of arsenic and lead in soils from the Butte, Montana, mining district. Environ Sci Technol 26(3):461–468. https://doi.org/10.1021/es00027a002

Davis A, Sellstone C, Clough S, Barrick R, Yare B (1996) Bioaccumulation of arsenic, chromium and lead in fish: constraints imposed by sediment geochemistry. Appl Geochem 11(3):409–423. https://doi.org/10.1016/0883-2927(95)00012-7

Davis A, Chappell RC, Olsen RL (1988) The use and abuse of Eh measurements. Are they meaningful in natural waters? In: Proc, National Water Well Association Ground Water Geochemistry Symp, National Water Well Assoc, pp 199–216

Diez-Ercilla M, Sánchez-España J, Yusta I, Wendt-Potthoff K, Koschorreck M (2014) Formation of biogenic sulfdes in the water column of an acidic pit lake: biogeochemical controls and effects on trace metal dynamics. Biogeochem 121(3):519–536. https://doi.org/10.1007/s10533-014-0020-0

Diez-Ercilla M, Falagan C, Yusta I, Sánchez-España J (2019) Metal mobility and mineral transformations driven by bacterial activity in acidic pit lake sediments: evidence from column experiments and sequential extraction. J Soils Sediments 19:1527–1542. https://doi.org/10.1007/s11368-018-2112-2

Drever JI (1982) The geochemistry of natural waters. The Prentice-Hall, Englewood Cliffs

Dzombak DA, Morel FMM (1990) Surface Complexation Modeling: Hydrous Ferric Oxide. Wiley, New York

Eary EL (1999) Geochemical and equilibrium trends in mine pit lakes. Appl Geochem 14(8):963–987. https://doi.org/10.1016/S0883-2927(99)00049-9

EPA (1996) Method 6010C inductively coupled plasma-atomic emission spectrometry. U.S. Environmental Protection Agency

Gaines RV, Skinner HCW, Foord EE, Mason B, Rosenzweig A (1997) Dana's new mineralogy. Wiley, New York

Gammons CH, Duaime TE (2006) Long term changes in the limnology and geochemistry of the Berkeley pit lake, Butte, Montana. Mine Water Environ 25:76–85. https://doi.org/10.1007/s10230-006-0114-6

Hamzaoui A, Mgaidi A, Megriche A, Maaoui ME (2002) Kinetic study of goethite formation from ferrihydrite in alkaline

medium. Ind Eng Chem Res 41(21):5226–5231. https://doi.org/10.1021/ie010931z
Holley EA, Lowe JA, Johnson CA, Pribil MJ (2019) Magmatic-hydrothermal gold mineralization at the Lone Tree Mine, Battle Mountain District. Nevada Econ Geol 114(5):811–856. https://doi.org/10.5382/econgeo.4665
Jones AM, Collins RN, Waite TD (2011) Mineral species control of aluminum solubility in sulfate-rich acidic waters. Geochim Cosmochim Acta 75(4):965–977. https://doi.org/10.1016/j.gca.2010.12.001
Kinniburgh DG, Jackson ML, Syers JK (1976) Adsorption of alkaline earth, transition, and heavy metal cations by hydrous oxide gels of iron and aluminum. Soil Sci Soc Am J 40(5):796–799. https://doi.org/10.2136/sssaj1976.03615995004000050047x
Koubeck E (1999) Gelatinous aluminum hydroxide. J Chem Ed 76:756. https://doi.org/10.1021/ed076p756.1
Langmuir D (1971) The geochemistry of some carbonated groundwaters in central Pennsylvania. Geochim Cosmochim Acta 35(10):1023–1045. https://doi.org/10.1016/0016-7037(71)90019-6
Langmuir D (1997) Aqueous environmental geochemistry. The Prentice-Hall Inc, Upper Saddle River
Leckie JO, Benjamin MM, Hayes K, Kaufman G, Altmann S (1980) Adsorption/coprecipitation of trace elements from water with iron oxyhydroxide. EPRI CS-1513 Project 910-1. Prepared for Electric Power Research Institute, Palo Alto
Li H-C, Ku T-H, Stott LD (1997) Stable isotope studies on Mono Lake (California). 1. ∂18O in lake sediments as proxy for climatic change during the last 150 years. Limnol Oceanogr 42(2):230–238. https://doi.org/10.4319/lo.1997.42.2.0230
Lindsay WL, Walthall PM (1995) The solubility of aluminum in soils. In: Sposito G (ed) The environmental chemistry of aluminum. Lewis Publishers, New York, pp 333–361
Lydersen E (1990) The solubility and hydrolysis of aqueous aluminum hydroxides in dilute fresh waters at different temperatures. Hydrol Res 21(3):195–204. https://doi.org/10.2166/nh.1990.0015
Meier J, Babenzien H, Wendt-Potthoff K (2004) Microbial cycling of iron and sulfur in sediments of acidic and pH-neutral mining lakes in Lusatia (Brandenburg, Germany). Biogeochem 67:135–156. https://doi.org/10.1023/B:BIOG.0000015324.22890.b7
Miller GC, Lyons WB, Davis A (1996) Understanding the water quality of pit lakes. Environ Sci Technol 30(3):118A-123A. https://doi.org/10.1021/es9621354
Murad E, Rojik P (2005) Iron mineralogy of mine-drainage precipitates as environmental indicators: review of current concepts and a case study from the Sokolov Basin. Czech Republic Clay Miner 40(4):427–440. https://doi.org/10.1180/0009855054040181
NDEP (2021) Guidance for Geochemical Modeling at Mine Sites. Nevada Division of Environmental Protection, Carson City, Nevada. https://ndep.nv.gov/uploads/land-mining-regs-guidance-docs/20210521_Geochem_GuidanceRev00_ADA.pdf. Accessed 3 Jan 2024
NDEP (2022) Guidance Document Waste Rock, Overburden, and Ore Characterization and Evaluation. Nevada Division of Environmental Protection. Carson City, Nevada. https://ndep.nv.gov/uploads/land-mining-regs-guidance-docs/20220630_GuidncDoc_WasteOvrbrdnOre_Char_ADA.pdf. Accessed 3 Jan 2024
Newman CP (2020) A quantitative framework for comparing observed and simulated pit lake geochemistry. Mine Water Environ 39:630–646. https://doi.org/10.1007/s10230-019-00634-0
Nordstrom DK (1982) The effects of sulfate on aluminum concentrations in natural waters: some stability relations in the system Al_2-SO_3 -H_2O at 298K. Geochim Cosmochim Acta 46(4):681–692. https://doi.org/10.1016/0016-7037(82)90168-5
Nordstrom DK (2020) Geochemical modeling of iron and aluminum precipitation during mixing and neutralization of acid mine drainage. Minerals 10(6):547–559. https://doi.org/10.3390/min10060547
Nordstrom DK, Nicholson A (2017) Geochemical modeling for mine site characterization and remediation. In: Soc for mining, metallurgy, and exploration
Nordstrom DK (2009) Pitfalls and limitations of mineral equilibrium assumptions for geochemical modeling of water-rock interactions at mine sites. In: Proc, 8th International Conf on Acid Rock Drainage, Skellefteå, Sweden
Oral CM, Ercan B (2018) Influence of pH on morphology, size and polymorph of room temperature synthesized calcium carbonate particles. Powder Tech 339:781–788. https://doi.org/10.1016/j.powtec.2018.08.066
Papadopoulos P, Rowell DL (2006) The reactions of cadmium with calcium carbonate surfaces. J Soil Sci 39:23–36. https://doi.org/10.1111/j.1365-2389.1988.tb01191.x
Paquette J, Reeder RJ (1995) Relationship between surface structure, growth mechanism, and trace element incorporation in calcite. Geochim Cosmochim Acta 59(4):735–749. https://doi.org/10.1016/0016-7037(95)00004-J
Parkhurst DL, Appelo CAJ (1999) User's guide to PHREEQC (version 2)—A computer program for speciation, batch-reaction, one-dimensional transport, and inverse geochemical modeling. U.S. Geological Survey, Denver
Petrash DA, Jan J, Sirova D, Osafo NOA, Borovec J (2018) Iron and nitrogen cycling, bacterioplankton community composition and mineral transformations involving phosphorus stabilization in the ferruginous hypolimnion of a post-mining lake. Environ Sci Process Impacts 20:1414–1426. https://doi.org/10.1039/C8EM00328A
Petrash DA, Steenbergen IM, Valero A, Meador TB, Paces T, Thomazo C (2022) Aqueous system-level processes and prokaryote assemblages in the ferruginous and sulfate-rich bottom waters of a post-mining lake. Biogeosciences 19(6):1723–1751. https://doi.org/10.5194/bg-19-1723-2022
Plummer LN, Wigley TML (1976) The dissolution of calcite in CO_2-saturated solutions at 25°C and 1 atmosphere total pressure. Geochim Cosmochim Acta 40(2):191–202. https://doi.org/10.1016/0016-7037(76)90176-9
Reeder RJ (1996) Interaction of divalent cobalt, zinc, cadmium and barium with the calcite surface during layer growth. Geochim Cosmochim Acta 60(9):1543–1552. https://doi.org/10.1016/0016-7037(96)00034-8
Regenspurg S, Brand A, Peiffer S (2004) Formation and stability of schertmannite in acidic mining lakes. Geochim Cosmochim Acta 68(6):1185–1197. https://doi.org/10.1016/j.gca.2003.07.015
Rothberg D. (2023) Bill seeking to avoid mining pit lakes advances in Legislature. The Nevada Independent. April 19. https://thenevadaindependent.com/article/bill-seeking-to-avoid-mining-pit-lakes-advances-in-legislature. Accessed 20 Mar 2024
Sánchez-España J, Yusta I (2019) Coprecipitation of Co^{2+}, Ni^{2+} and Zn^{2+} with Mn(III/IV) oxides formed in metal-rich mine waters. Minerals 9:226–248. https://doi.org/10.3390/min9040226
Sánchez-España J, Pamo EL, Santofimia E, Aduvire O, Reyes J, Barettino D (2005a) Acid mine drainage in the Iberian Pyrite Belt (Odiel River watershed, Huelva, SW Spain): geochemistry, mineralogy and environmental implications. Appl Geochem 20:1320–1356. https://doi.org/10.1016/j.apgeochem.2005.01.011
Sánchez-España J, Pamo EL, Pastor ES, Andres JR, Rubi JAM (2005b) The natural attenuation of two acidic effluents in

Tharsis and La Zarza-Perrunal mines (Iberian Pyrite Belt, Huelva, Spain). Environ Geol 49(2):253–266. https://doi.org/10.1007/s00254-005-0083-2

Sánchez-España J, Pamo EL, Pastor ES, Ercilla MD (2008) The acidic mine pit lakes of the Iberian Pyrite Belt: an approach to their physical limnology and hydrogeochemistry. Appl Geochem 23(5):1260–1287. https://doi.org/10.1016/j.apgeochem.2007.12.036

Sánchez-España J, Pamo EL, Diez M, Santofimia E (2009) Physico-chemical gradients and meromictic stratification in Cueva de la Mora and other acidic pit lakes of the Iberian Pyrite Belt. Mine Water Environ 28:15–29. https://doi.org/10.1007/s10230-008-0059-z

Sánchez-España J, Yusta I, Diez-Ercilla M (2011) Schwertmannite and hydrobasaluminite: a re-evaluation of their solubility and control on the iron and aluminium concentration in acidic pit lakes. Appl Geochem 26:1752–1774. https://doi.org/10.1016/j.apgeochem.2011.06.020

Sánchez-España J, Yusta I, López GA (2012) Schwertmannite to jarosite conversion in the water column of an acidic mine pit lake. Mineral Mag 76:2959–2682. https://doi.org/10.1180/minmag.2012.076.7.03

Sánchez-España J, Yusta I, Gray J, Burgos WD (2016) Geochemistry of dissolved aluminum at low pH: extent and significance of Al-Fe (III) coprecipitation below pH 4.0. Geochim Cosmochim Acta 175:128–149. https://doi.org/10.1016/j.gca.2015.10.035

Sánchez-España J, Yusta I, Ilin A, van der Graaf C, Sánchez-Andrea I (2020) Microbial geochemistry of the acidic saline Pit Lake of Brunita Mine (La Unión, SE Spain). Mine Water Environ 39:535–555. https://doi.org/10.1007/s10230-020-00655-0

Savage K, Ashley RP, Bird DK (2009) Geochemical evolution of a high arsenic alkaline pit-lake in the Mother Lode Gold District, California. Econ Geol 104:1171–1211. https://doi.org/10.2113/gsecongeo.104.8.1171

Schafer WM, Croall J, Schmidt J (2020) Predicting water quality trends in Lone Tree pit lake, Nevada (USA). Mine Water Environ 39:618–629. https://doi.org/10.1007/s10230-020-00698-3

Schwertmann U, Murad E (1983) Effect of pH on the formation of goethite and hematite from ferrihydrite. Clays Clay Miner 31:277–284. https://doi.org/10.1346/CCMN.1983.0310405

Smith KS (1991) Factors influencing metal sorption onto iron-rich sediment in acid-mine drainage. PhD Diss Colorado School of Mines, Golden, Colorado

Story S, Bowen BB, Benison KC, Schulze DG (2010) Authigenic phyllosilicates in modern acid saline lake sediments and implications for Mars. J Geophys Res 115:E12012–E12029. https://doi.org/10.1029/2010JE003687

Swallow KC, Hume DN, Morel FMM (1980) Sorption of copper and lead by hydrous ferric oxide. Environ Sci Technol 14(11):1326–1331. https://doi.org/10.1021/es60171a003

Takahashi T (1960) Supergene alteration of zinc and lead deposits in limestone. Econ Geol 55:1083–1115. https://doi.org/10.2113/gsecongeo.55.6.1083

Twidwell LG, Gammons CH, Young CA, Berg RB (2006) Summary of deepwater sediment/pore water characterization for the metal-laden Berkeley Pit Lake in Butte, Montana. Mine Water Environ 25:86–92. https://doi.org/10.1007/s10230-006-0115-5

van Breeman N (1973) Dissolved aluminum in acid sulfate soils and in acid mine waters. Soil Sci Soc Am Proc 37:694–697. https://doi.org/10.2136/sssaj1973.03615995003700050020x

van der Graaf CM, Sánchez-España J, Yusta I, Ilin A, Shetty SA, Bale NJ, Villanueva L, Stams AJM, Sánchez-Andrea I (2020) Biosulfidogenesis mediates natural attenuation in acidic mine pit lakes. Microorganisms 8(9):1275–1301. https://doi.org/10.3390/microorganisms8091275

Waychunas GA, Rea BA, Fuller CC, Davis JA (1993) Surface chemistry of ferrihydrite: Part 1. EXAFS studies of the geometry of coprecipitated and adsorbed arsenate. Geochim Cosmochim Acta 57(10):2251–2269. https://doi.org/10.1016/0016-7037(93)90567-G

Yee N, Shaw S, Benning LG, Nguyen TH (2006) The rate of ferrihydrite transformation to goethite via the Fe(II) pathway. Am Mineral 91:92–96. https://doi.org/10.2138/am.2006.1860

Younger PL, Banwart SA, Hedin RS (2002) Mine water: hydrology, pollution, remediation. Kluwer Academic Publishers, Dordrecht